Inter-membrane association of the Sec and BAM translocons for bacterial outer-membrane biogenesis

Sara Alvira[1*], Daniel W. Watkins[1*], Lucy Troman[1], William J. Allen[1], James Lorriman[1], Gianluca Degliesposti[2], Eli J. Cohen[3], Morgan Beeby[3], Bertram Daum[4], Vicki A.M. Gold[4], J. Mark Skehel[2] and Ian Collinson[1†]

[1], *School of Biochemistry, University of Bristol, BS8 1TD, United Kingdom*

[2], *Biological Mass Spectrometry and Proteomics, MRC Laboratory of Molecular Biology, Francis Crick Avenue, Cambridge, CB2 0QH, United Kingdom*

[3], *Faculty of Natural Sciences, Department of Life Sciences, Imperial College, London SW7 2AZ, United Kingdom*

[4], *Living Systems Institute, University of Exeter, EX4 4QD, United Kingdom*

[*], these authors contributed equally to this work

[†], corresponding author: ian.collinson@bristol.ac.uk

SUMMARY (150/ 150)

The outer-membrane of Gram-negative bacteria is critical for surface adhesion, pathogenicity, antibiotic resistance and survival. The major constituent – hydrophobic β-barrel Outer-Membrane Proteins (OMPs) – are secreted across the inner-membrane through the Sec-translocon for delivery to periplasmic chaperones *e.g.* SurA, which prevent aggregation. OMPs are then offloaded to the β-Barrel Assembly Machinery (BAM) in the outer-membrane for insertion and folding. We show the Holo-TransLocon (HTL: an assembly of the protein-channel core-complex SecYEG, the ancillary sub-complex SecDF, and the membrane 'insertase' YidC) contacts SurA and BAM through periplasmic domains of SecDF and YidC, ensuring efficient OMP maturation. Our results show the trans-membrane proton-motive-force (PMF) acts at distinct stages of protein secretion: for SecA-driven translocation across the inner-membrane through SecYEG; and to communicate conformational changes *via* SecDF to the BAM machinery. The latter presumably ensures efficient passage of OMPs. These interactions provide insights of inter-membrane organisation, the importance of which is becoming increasingly apparent.

32

33 **INTRODUCTION**

34 Outer-membrane biogenesis in Gram-negative bacteria (reviewed in (Konovalova et al.,
35 2017)) requires substantial quantities of protein to be exported; a process which begins by
36 transport across the inner plasma membrane. Precursors of β-barrel Outer-Membrane Proteins
37 (OMPs) with cleavable N-terminal signal-sequences are targeted to the ubiquitous Sec-
38 machinery and driven into the periplasm by the ATPase SecA and the trans-membrane proton-
39 motive-force (PMF) (Brundage et al., 1990; Collinson, 2019; Cranford-Smith and Huber, 2018;
40 Lill et al., 1989). Upon completion, the pre-protein signal-sequence is proteolytically cleaved
41 (Chang et al., 1978; Josefsson and Randall, 1981), releasing the mature unfolded protein into
42 the periplasm. The emergent protein is then picked up by periplasmic chaperones, such as SurA
43 and Skp, which prevent aggregation (McMorran et al., 2013; Sklar et al., 2007), and somehow
44 facilitate delivery to the β-Barrel Assembly Machinery (BAM) for outer-membrane insertion
45 and folding (Voulhoux et al., 2003; Wu et al., 2005).

46 In *E. coli,* BAM consists of a membrane protein complex of subunits BamA-E, of known
47 structure (Bakelar et al., 2016; Gu et al., 2016; Iadanza et al., 2016). The core component,
48 BamA, is a 16 stranded β-barrel integral membrane protein, which projects a large periplasmic
49 stretch of 5 POlypeptide TRanslocation-Associated (POTRA) domains into the periplasm.
50 BamB-E are peripheral membrane lipoproteins anchored to the inner leaflet of the OM. Despite
51 structural insights, the mechanism for BAM-facilitated OMP insertion is unknown (Ricci and
52 Silhavy, 2019).

53 The bacterial periplasm is a challenging environment for unfolded proteins, so complexes
54 spanning both membranes are critical for efficient delivery through many specialised secretion
55 systems (Green and Mecsas, 2016). So, how do enormous quantities of proteins entering the
56 periplasm *via* the general secretory pathway (Sec) efficiently find their way through the cell
57 envelope to the outer-membrane? From where is the energy derived to facilitate these
58 trafficking processes some distance from the energy transducing inner-membrane and in an
59 environment lacking ATP? Could it be achieved by a direct interaction between chaperones,
60 and the translocons of the inner (Sec) and outer (BAM) membranes?

61 The core-translocon, SecYEG, does not possess periplasmic domains of sufficient size to
62 mediate such an interaction (Van den Berg et al., 2004). However, the Holo-TransLocon (HTL)

63 contains the ancillary sub-complex SecDF and the membrane protein 'insertase' YidC (Duong
64 and Wickner, 1997; Schulze et al., 2014); both of which contain periplasmic extensions
65 potentially large enough to reach the POTRA domains of BamA.

66 SecDF is a member of the so called Root Nodulation Division (RND) superfamily of proton-
67 motive-force (PMF) driven transporters (reviewed in (Tseng et al., 1999)). It is a highly
68 conserved component of the bacterial Sec translocon, where it has long been known to facilitate
69 protein secretion (Duong and Wickner, 1997; Economou et al., 1995; Pogliano and Beckwith,
70 1994). While fellow component of the HTL – YidC – is essential for membrane protein
71 insertion, and thus indispensable (Samuelson et al., 2000; Scotti et al., 2000), knock out mutants
72 of *secD* and *secF* are not fatal but severely compromised and cold-sensitive (Gardel et al.,
73 1987), presumably due to deficiencies in envelope biogenesis. The cause of this has been
74 ascribed to a defect in protein transport across the inner membrane.

75 In keeping with other members of the RND family, like AcrB (Eicher et al., 2014), SecDF
76 confers PMF stimulation of protein secretion (Arkowitz and Wickner, 1994). Different
77 structures of SecDF show the large periplasmic domains in different conformational states
78 (Furukawa et al., 2018; Kumazaki et al., 2014; Mio et al., 2014), also affected by altering a key
79 residue of the proton transport pathway ($SecD_{D519N}$ – *E. coli* numbering) (Furukawa et al.,
80 2017). On this basis, an elaborate mechanism has been proposed whereby PMF driven
81 conformational changes at the outer surface pick up and pull polypeptides as they emerge from
82 the protein channel exit site of SecY. Yet, ATP- and PMF-driven translocation across the inner
83 membrane does not require SecDF or YidC (Gardel et al., 1987; Schulze et al., 2014); SecYEG
84 and SecA will suffice (Brundage et al., 1990). Evidently then, there must be two PMF-
85 dependent components of protein secretion: one early stage dependent on SecYEG/ SecA, and
86 another later event on AcrB-like SecDF activity. This distinction has not been fully considered.

87 This study explores the role of the ancillary components of the Sec machinery for protein
88 secretion and downstream trafficking through the periplasm for outer-membrane delivery and
89 maturation. In particular, we examine the possibility of a direct interaction between the HTL
90 and BAM machineries to facilitate protein transport through the envelope. The basic properties
91 and structure of the inter-membrane super-complex are investigated, as well as its importance
92 for OMP folding and insertion. The implications of this interaction and its modulation caused
93 by proton transport through SecDF are profound. Thus, we consider their consequences for the

94 mechanism of protein transport through the Sec and BAM machineries, and for outer-
95 membrane biogenesis.
96
97
98 **RESULTS**
99
100 **Co-fractionation and immunoprecipitation highlight an interaction between the Sec and**
101 **BAM machineries**
102 Total *E. coli* membranes of cells over-producing either SecYEG or HTL were prepared and
103 fractionated by sucrose gradient centrifugation to separate the inner- and outer-membranes (Fig.
104 1a). We first sought to determine the precise locations of IM and OM proteins in the fractions;
105 SDS-PAGE analysis of the fractions stained for total protein revealed the presence of SecY in
106 the lighter inner-membrane fractions (Fig. S1a, asterisk – left panel). Heating the fractions
107 (required to unfold outer membrane proteins) prior to SDS-PAGE helped reveal the location of
108 the most highly expressed outer membrane residents (OmpC and OmpF; Fig. S1a, asterisk –
109 right panel). Thus, in these gradients fraction 1-3 mostly contain outer-membranes, and
110 fractions 4-6 are composed mainly of inner-membranes.
111 Immunoblotting confirmed the presence of the BAM components (BamA, BamB and
112 BamD), as expected, in OM fractions (OM; Fig. 1b). Likewise, the over-produced SecY and
113 SecE subunits mark the fractions containing the core-complex (SecYEG) in the IM fractions
114 (IM; Fig. 1b, YEG↑). However, when over-produced as part of HTL there is a marked shift of
115 their migration towards the outer-membrane containing fractions (Fig. 1b, HTL↑).
116 Interestingly, the over-production of SecDF alone results in a similar effect (Fig. 1c); a
117 measurable increase of SecY and SecG in the outer-membrane containing fractions. This effect
118 was lost in comparable experiments where the periplasmic domain of SecD (P1) had been
119 removed (Fig. 1c). Our interpretation of these experiments is that the interaction between the
120 Sec and Bam complexes, requiring at least the periplasmic domains of SecD (and most likely
121 SecF and YidC), causes an association of inner and outer membrane vesicles reflected in the
122 shift we observe.
123 To further examine this interaction, we extracted native membranes with a mild detergent
124 for Immuno-Precipitation (IP) using a monoclonal antibody raised against SecG. The pull-

125 downs were then probed for native interacting partners by western blotting (Fig. 1d,e, Fig. S1b).
126 As expected, SecG (positive control) and SecD of HTL co-immuno-precipitated. Crucially,
127 BamA could also be detected. The specificity of the association was demonstrated by controls
128 omitting the SecG antibody or the SecG protein (produced from membranes extracts of a *ΔsecG*
129 strain (Nishiyama et al., 1994)), wherein non-specific binding was either undetectable, or
130 considerably lower than the specific co-immuno-precipitant (Fig. 1d). When BAM was over-
131 produced, the yield of BamA recovered in the IPs increased accordingly (Fig. 1d, e, Fig. S1b).
132 In a similar experiment, a hexa-histidine tagged BamA was used to isolate BAM from cells
133 over-producing the complex. Western blots showed that BamA co-purified, as expected, with
134 additional components of the BAM complex (BamB and BamD), and crucially also with SecD
135 and SecG of the HTL (Fig. 1f, Fig. S1c). Again, controls (omitting Ni^{2+}, or recombinant his_6-
136 BamA) were reassuringly negative.
137
138 **Interaction between HTL and BAM is cardiolipin dependent**
139 The phospholipid CardioLipin (CL) is known to be intimately associated with energy
140 transducing systems, including the Sec-machinery, for both complex stabilisation and efficient
141 transport (Corey et al., 2018; Gold et al., 2010; Schulze et al., 2014). For this reason, the IP
142 experiments above were augmented with CL. On omission of CL the interactions of SecG with
143 SecD and BamA were reduced ~ 3- and 5-fold, respectively (Fig. 1d, e; Fig. S1b). This lipid-
144 mediated enhancement of the SecG-SecD interaction is consistent with our previous finding
145 that CL stabilises HTL (Schulze et al., 2014), and shows it also holds true for the HTL-BAM
146 interaction. *Apropos*, CL has been shown to be associated with the BAM complex (Chorev et
147 al., 2018).
148
149 **HTL and BAM interact to form an assembly large enough to bridge the inner and outer**
150 **membranes**
151 To confirm the interaction between the Sec and BAM machineries, the purified complexes
152 were subjected to glycerol gradient centrifugation. When mixed together, HTL and BAM co-
153 migrated towards higher glycerol concentrations, beyond those attained by the individual
154 complexes (Fig. 2a); consistent with the formation of a larger complex due to an interaction
155 between the two. The interaction is clear, but not very strong, likely due to the required transient

156 nature of the association between the two translocons *in vivo*, and also because of the complete
157 breakdown of the inner and outer membranes by detergent – required for this experiment. When
158 the experiment was repeated with the individual constituents of HTL: SecDF and YidC, but not
159 SecYEG, were also shown to interact with BAM (Fig. S2a-c).

160 Visualisation of the heavy fractions containing interacting HTL and BAM by Negative Stain
161 (NS)-Electron Microscopy (EM) revealed a heterogeneous mixture of small and very large
162 complexes (Fig. S3a, large complexes marked with white arrows). As noted above, this mixed
163 population is probably due to the expected transient nature of the interaction between the two
164 complexes, and/ or due to super-complex instability caused by loss of the bilayer and
165 specifically bound phospholipids, *e.g.* CL, during purification (see above and below). Even
166 though we augment the material with CL it is unlikely the full complement of native lipids
167 found in the membrane bound state are restored.

168 To overcome this heterogeneity we stabilised the complex by cross-linking, using GraFix
169 (Kastner et al., 2008) (Fig. S4a, middle). Note that this interaction was also demonstrated by
170 size exclusion chromatography, performed for sample preparation for mass spectrometry and
171 cryo-EM (see below). Visualisation by NS-EM revealed a marked reduction in the number of
172 dissociated complexes (Fig. S3b). As expected, omitting CL from the preparation resulted in
173 dissociation of the majority of the large complexes, even with GraFix (Fig. S3c), supporting the
174 findings above of the CL dependence of the interaction (Fig. 1e).

175 Mass spectrometry confirmed the presence of BAM and HTL constituents in a high
176 molecular weight GraFix fraction (Fig. S4a, right; Table S1), which was selected for analysis
177 by NS-EM. The subsequent single particle analysis of this material (Table S2) revealed a
178 remarkable structure large enough (~ 300 x 250 x 150 Å) to contain both Sec and BAM
179 machineries (Botte et al., 2016; Iadanza et al., 2016), and with a height sufficient to straddle the
180 space between the two membranes (Fig. 2b, Fig. S4b), especially when considering the
181 plasticity of the periplasm (Zuber et al., 2008). Moreover, the periplasmic domains of the HTL
182 and BAM complexes are potentially large enough reach out across the space between the inner
183 and outer-membranes to contact one another. Indeed, regions of SecDF and the POTRA
184 domains of BamA have been show to extend ~ 60 Å (Furukawa et al., 2017) and ~ 110 Å (Ma
185 et al., 2019) respectively, sufficient to bridge this gap.

186 To assign the locations and orientations of the individual constituents of HTL and BAM, we
187 compared the 3D reconstructions of different sub-complexes: BAM bound to SecYEG-DF
188 (without YidC) (Fig. S4c) or SecDF alone (Fig. S4d). The difference analysis revealed the
189 locations of YidC (Fig. 2b, pink; Fig. S4c, pink arrow), SecDF (Fig. 2b, green; Fig. S4d, green
190 arrow) and SecYEG (Fig. 2b, blue; Fig. S4d, blue arrow) at the bottom of the assembly
191 (assigned as the inner-membrane region). The orientation of BAM relative to SecDF is different
192 in SecDF-BAM compared to HTL-BAM (Fig. S4d, red arrows), possibly due to its known
193 ability to move (see below), and/ or the absence of stabilising interactions with the rest of HTL
194 components.
195 Removing BamB from the complex results in the loss of significant mass in the area
196 designated as the OM region with respect to the holo-structure (Fig. 2b, orange; Fig. S4e, orange
197 arrow). This confirmed the orientation of the inner and outer-membranes, and the assignment
198 of the BAM complex as shown in Fig. 2b. Interestingly, the complex lacking BamB shows a
199 diminishment of the density assigned as YidC (Fig. S4e, pink arrow), suggestive of a mutual
200 interaction between the two.
201
202 **Periplasmic domains of the Sec and BAM translocons associate to form a large cavity**
203 **between the bacterial inner and outer membranes**
204 Despite heterogeneity in the sample we were able to isolate a cross-linked HTL-BAM
205 complex by size exclusion chromatography and produce a low-resolution cryo-EM structure
206 (Fig. 2c, Fig. S5 and Table S2) with an overall resolution of 18.23 Å.Taken together with the
207 difference map generated by NS-EM (Fig. 2b; Fig. S4) the structure reveals the basic
208 architecture of the assembly and the arrangement of constituent subunits.
209 The extreme complexity of the image processing resulted in an insuffient number of particles
210 to attain high resolution. Many factors contribute to this problem: the dynamism of the complex,
211 due to the limited contact surface between the HTL and BAM; its inherent mobility necessary
212 for function; the presence of detergent surrounding the trans-membrane regions of the HTL and
213 BAM components, accounting for most of the surface of the assembly; and finally, the absence
214 of inner- and outer-membranes scaffolds. The loss of the fixed double membrane architecture
215 was particularly problematic; during image processing we found different sub-populations

216 where the BAM pivots away from its raised position towards where the inner membrane would
217 otherwise have been. Obviously, this would not happen if restrained by the outer-membrane.
218 In spite of all this, the attainable structure proved to be very illuminating. Due to the limited
219 resolution, we deployed cross-linking mass spectroscopy (XL-MS) to verify the contacts
220 between HTL and BAM responsible for inter-membrane contact points. The HTL and BAM
221 complexes were mixed together in equimolar quantities and cross-linked with the lysine-
222 specific reagent DSBU. The reaction mixture was then fractionated by gel filtration and
223 analysed by SDS-PAGE. A single band corresponding to the cross-linked HTL-BAM complex
224 was detected (Fig. S6a); note that the isolation of the intact HTL-BAM complex by size
225 exclusion chromatography provides further evidence of a genuine interaction. The fractions
226 containing the cross-linked complex were combined and digested before LC-MS/ MS analysis.
227 The analysis of mass spectrometry data enabled the detection and mapping of the inter- and
228 intra-molecular protein cross-links within the assembly. The results show an intricate network
229 of interactions most of which are consistent with the cryo-EM structure, particularly at one side
230 of the assembly between SecD and BamBCD, and on the other side between YidC and
231 BamABCD (Fig. S6b,c). All the constituent proteins of HTL were cross-linked to BAM
232 subunits with exception of SecG and YajC. Thus, the resulting co-immunoprecipitation and
233 affinity pull down of SecG with the Bam components (described above; Fig. 1d-f) must have
234 been the result of an indirect interaction, presumably *via* SecDF-YidC. This is consistent with
235 the lack of an interaction of SecYEG alone and the BAM complex (Fig. S2b), and the
236 assignment of the electron microscopy structures (Fig. 2b,c) – showing no connection between
237 SecYEG and BAM. In this respect, it is interesting to note in the structure that the periplasmic
238 domains of SecD, YidC and to a lesser degree SecF, extend to establish multiple interactions
239 with the BAM lipoproteins suggesting a pivotal role for these subunits in the formation of the
240 HTL:BAM complex (Fig. 2c,e). This bridge between the two complexes also helps to define a
241 very large cavity between the IM and OM (Fig. 2d).
242 The BAM complex is recognisable in the cryo-EM structure at the outer membrane with the
243 expected extensive periplasmic protrusions (Bakelar et al., 2016; Gu et al., 2016). Some
244 components of the BAM complex, such as BamB, can be unambiguoulsy docked at the cryo-
245 EM structure, due to the direct determination by NS and its easily recognisable ß-propeller

246 shape (Fig. 2e). We suggest also the locations of BamA, BamC and BamD according to the
247 cryo-EM density and the constraints of the XL-MS data (Fig. 2e; Fig. S6c).
248 The inner-membrane region the HTL is much more open than the previous structure, when
249 visualised alone (Botte et al., 2016). In the new open structure, the locations of the core-
250 complex SecYEG, SecDF and YidC can be easily distinguished, connected by two bridges from
251 the former (Fig. 2f, left, asterisks). These bridging sites could be the binding sites of CL and
252 the central lipid pool identified previously, required for structural stability and translocon
253 activity (Corey et al., 2018; Martin et al., 2019; Schulze et al., 2014). Within SecYEG the
254 protein channel can be visualised though the centre, along with the lateral gate (required for
255 signal sequence binding and inner membrane protein insertion) facing towards SecDF, YidC
256 and the putative central lipid pool (Martin et al., 2019; Fig. 2f, right).
257
258 **Cardiolipin, required for super-complex formation, stabilises an 'open' form of the HTL**
259 The HTL bound to BAM in our EM structure (Fig. 3a, structure ii) seems to be more open
260 when compared to the previously published low-resolution cryo-EM structure (Botte et al.,
261 2016) (emd3056; Fig. 3a, structure i), and also displays a more prominent periplasmic region.
262 Preparations of HTL alone, made in this study, contain both a 'compact' state (Fig. 3a, structure
263 iii) similar to that of the previously published structure (Fig. 3a, structure i), as well as a
264 proportion of an 'open' state, with proud periplasmic domains, not previously described (Fig.
265 3a, structure iv), and apparently more similar to that seen in the HTL-BAM structure (Fig. 3a,
266 structure ii).
267 The HTL sample used here is extremely pure, of known subunit composition and not prone
268 to oligomerisation (Schulze et al., 2014). So, we can rule out that this larger form, assigned as
269 an 'open' state, of HTL is not due to the presence of contaminants, unknown additional partner
270 proteins, or dimerisation. Instead, the reason for the presence of these different populations –
271 'compact' and 'open' states – is likely due to varying interactions with lipids, including CL.
272 Lipid content within the HTL is critical for proper structure and function, and CL is particularly
273 important for protein translocation through the Sec machinery (Corey et al., 2018; Gold et al.,
274 2010; Hendrick and Wickner, 1991; Schulze et al., 2014). Depletion of these core lipids, for
275 instance by detergent extraction, might be expected to cause a collapse of the complex.
276 Augmenting the HTL with CL during purification increased the proportion of the 'open' state

277 (from 8% to 17%), which could be enriched by glycerol gradient fractionation (to 32%), and
278 further stabilised by cross-linking (to 40%) (Fig. S7).
279 Evidently then, it seems likely that the open conformation (Fig. 3a, structure iv) is the state
280 capable of interacting with the BAM complex (Fig. 3a, structure ii). The 'open' structure, and
281 the 'compact' structure seen before (Botte et al., 2016), may reflect different functional states
282 of the translocon. Presumably, the HTL would be closed when idle in the membrane, and would
283 open to various degrees depending on the associated cytosolic partners (*e.g.* ribosomes or
284 SecA), periplasmic factors (chaperones, BAM, *etc*.) and various substrates. Thus, it is not
285 suprising that when free of the constraints of the membrane, and in the harsh environment of a
286 detergent micelle, that these various states can be adopted.
287
288 **Increasing the distance between inner and outer membranes weakens the HTL-BAM**
289 **interaction**
290 The dimensions of the HTL-BAM structure roughly corresponds to the distance between the
291 inner and outer membranes. Increasing the thickness of the periplasm might therefore be
292 expected to reduce formation of HTL-BAM complexes, as previously observed for other trans-
293 periplasmic complexes (Asmar et al., 2017; Cohen et al., 2017). To test this prediction, we
294 increased the thickness of the periplasm by manipulating the width-determining lipoprotein
295 Lpp, which separates the outer membrane from the peptidoglycan layer. Increasing the length
296 of *lpp* thus increases the width of the periplasm, from ~ 250 Å for wild-type *lpp* to ~ 290 Å
297 when an additional 21 residues are added to the resultant protein (Lpp_{+21}) (Asmar et al., 2017)
298 (Fig. 4a).
299 The experiments described above (Fig. 1d,e) were repeated: extracting total membranes in
300 the presence of CL for IP by antibodies raised against SecG. Blotting for SecD and BamA then
301 provided a measure respectively for interactions between HTL and BAM (Fig. 4b,c, Fig. S8) in
302 the lpp_{+21} background. Consistent with our model, the integrity of the HTL in the inner
303 membrane was unaffected, but the recovery of HTL-BAM was reduced more than 3-fold.
304
305 **PMF stimulation of protein translocation through the inner membrane by SecA and**
306 **SecYEG is not conferred by proton passage through SecD**

307 It has been known for many years that SecDF plays a critical role in protein secretion. The
308 results above show that the periplasmic domains of HTL, and in particular those of SecDF,
309 mediate the recruitment of the BAM complex, likely to facilitate the onward journey of proteins
310 to the outer membrane. Therefore, we decided to re-evaluate the precise role and activity of this
311 ancillary sub-complex. Experiments were established to investigate: (1) the role of SecDF in
312 SecA dependent protein transport through the inner membrane *via* SecYEG, and (2) the
313 consequences of its interaction with the BAM machinery for outer membrane protein
314 maturation. In particular, we set out to explore the possibility of an active role in these events
315 for the proton translocating activity of the SecDF sub-complex.

316 *secDF* null mutants exhibit a severe export defect, and are only just viable (Pogliano and
317 Beckwith, 1994). To explore this phenotype further we utilised *E. coli* strain JP325, wherein
318 the production of SecDF is under the control of an *ara* promoter: the presence of arabinose or
319 glucose, respectively results in production or depletion of SecDF-YajC (Economou et al., 1995)
320 (Fig. 5a, Fig. S9a). When plated, depletion of SecDF-YajC results in a strong growth defect
321 (Fig. 5b, panels 1 and 2), which can be rescued by recombinant expression of wild type *secDF*
322 (Nouwen and Driessen, 2002) (Fig. 5b, panels 3 and 4). In contrast, expression of $secD_{D519N}F$,
323 which results in the production of a complex defective in proton transport (Furukawa et al.,
324 2017), did not complement the defect (Fig. 5b, panels 5 and 6).

325 In light of these findings, we set up a classical *in vitro* transport assay investigating SecA-
326 driven proOmpA transport into inner membrane vesicles (IMVs) containing either over-
327 produced native HTL, or the defective version of HTL (containing $SecD_{D519N}F$). Both sets of
328 vesicles contained similar concentrations of SecY (Fig. S9b), yet despite the blocked proton
329 pathway through SecDF, there was no difference in the efficiencies of transport (Fig. 5c). The
330 lower quantities of transported pre-protein compared to the core-complex (SecYEG) most
331 likely reflects the reduced quantities of SecYEG in the HTL experiments, measured by blotting
332 for SecY (Fig. S9b).

333 Most importantly, the results demonstrate that HTL does not require a functional proton wire
334 through SecDF for SecA mediated ATP and PMF driven protein translocation (Fig. 5c). In this
335 respect, SecYEG and SecA are sufficient (Brundage et al., 1990). Therefore, the proton
336 translocating activity of SecD, crucial for cell survival, must be required for something else
337 other than secretion through the SecYEG core complex.

338

339 **Interaction between the Sec and BAM complexes is required for efficient OmpA folding**

340 The most obvious function of an interaction between the Sec and BAM machineries would
341 be to facilitate efficient delivery and insertion of OMPs to the OM. We therefore reasoned that
342 disrupting this interaction might compromise OMP delivery to BAM, leading to the
343 accumulation of unfolded OMPs in the periplasm – particularly where high levels of OM
344 biogenesis are required, such as in rapidly dividing cells. Elevated levels of unfolded OmpA
345 (ufOmpA) in the periplasm are a classical signature of OMP maturation deficiencies (Bulieris
346 et al., 2003; Sklar et al., 2007), and can be easily monitored by SDS-PAGE and western blotting:
347 folded OmpA (fOmpA) does not denature fully in SDS unless boiled, it therefore runs at a lower
348 apparent molecular mass on a SDS-PAGE compared to ufOmpA (Fig. 5d, left) (Bulieris et al.,
349 2003; Sklar et al., 2007).

350 Based on the above results, SecDF looks like the most important mediator of the Sec-BAM
351 interaction. We therefore used the SecDF depletion strain (JP325) as a basis for functional
352 assays. To overcome the growth defect (Fig. 5b, panels 1 and 2) and produce sufficient cells to
353 analyse, overnight cultures of the strains used above were grown in permissive media
354 (arabinose), and then transferred to new media containing glucose. At OD_{600nm} = 1.0, the
355 cultures were harvested and membranes were prepared and solubilised for analysis by co-IP as
356 described above. As expected, depletion of SecD (Fig. S9c-d) reduced pull down of BamA
357 (approximately 3-fold) compared to the complemented cells (Fig. 5e-f; Fig. S9c-d).

358 Overnight cultures were next prepared as described above, and then transferred to new media
359 containing either arabinose or glucose, marked as t = 0 in Fig. 5a, d, g-i. Samples were then
360 taken at regular intervals and the ratio of unfolded to folded OmpA determined (Fig. 5d, i),
361 along with cell density (Fig. 5h) and SecD levels (Fig. 5g). Under SecDF depletion conditions
362 (red squares), high levels of unfolded OmpA accumulate in the periplasm, particularly during
363 the exponential phase where the demand for OM biogenesis is very high (Fig. 5d, asterisk; Fig.
364 5h,i; Fig. S9e). Meanwhile, under permissive conditions (Fig. 5g-i, arabinose, yellow circles),
365 an increase in ufOmpA is observable after 1.5 h, but it recovers fully by 3 h. Notably, this
366 change is accompanied by a transient decrease in SecDF levels.

367 Clearly, the expression of *secDF* and levels of ufOmpA in the cell envelope are anti-
368 correlated, exacerbated during fast cell growth. These effects were not an indirect consequence

369 of BamA loss, which was unperturbed (Fig. S9f). Taken together, the data show that depletion
370 of SecDF reduces the interaction between HTL and BAM, and thereby hampering transport of
371 β-barrel proteins to the outer-membrane – resulting in a build-up of ufOmpA in the periplasm.
372 This would compromise the integrity of the outer-membrane and explain the cold-sensitivity of
373 *secDF* mutants (Gardel et al., 1987).
374

375 **Proton transport through SecD is required for efficient outer membrane protein**
376 **maturation**

377 Proton translocation through SecD is crucial for cell growth (Fig. 5b, panels 5 and 6), but
378 evidently not for PMF-stimulated transport through the inner membrane *via* SecYEG (Fig. 5c).
379 To determine if this activity is required for downstream events, we once again deployed the
380 SecDF depletion strain, complemented with wild-type or mutant *secDF* (as above, Fig. 5b,
381 panels 3 - 6). Comparable quantities of the respective SecD variants could be produced (Fig.
382 5g, green and purple; Fig. S9a). The defective HTL(SecD$_{D519N}$F) protein retained its ability to
383 interact with the BAM complex (Fig. 5f; Fig. S9c,d). The analysis showed the wild type, but
384 not the mutant, reduced unfolded OmpA in the periplasm to levels much closer to that of the
385 strain grown in permissive conditions (Fig. 5i; green and purple, respectively; Fig. S9e).
386 Therefore, proton transport through SecDF is apparently required for efficient outer membrane
387 protein folding.
388

389 **HTL(SecD$_{D519N}$F) adopts a different conformation to the native version**

390 The PMF-dependent mobility of the periplasmic domain of SecD (Furukawa et al., 2017)
391 may be critical for its activity as part of the BAM-HTL complex. To test this, the variant of
392 HTL containing SecD$_{D519N}$ was produced for comparison with the native form. Electron
393 microscopy was used to assess the extent of the 'compact' and 'open' forms of the HTL
394 complex (Fig. 5j, respectively structures i and ii). The 2D classification of HTL-SecD$_{D519N}$
395 shows the open state is populated to a similar extent compared to the unmodified HTL (Fig.
396 S10).

397 The 3D analysis shows the compact states in both cases, similar to those seen before (Botte
398 et al., 2016) (Fig. 3, structure i; Fig. 5j, structures i and iv). However, the 'open' states are
399 significantly different: blocking the proton pathway in SecD results in a shorter extension of

400 the periplasmic domains of the HTL, compared to the unmodified form (Fig. 5j, structures ii
401 *versus* v). This is consistent with the conformational change observed at atomic resolution in
402 SecDF alone (Fig. 5j, structures iii *versus* vi) (Furukawa et al., 2017). Even at the current low-
403 resolution description of the HTL-BAM complex (Fig. 2), it is clear that these observed PMF-
404 dependent conformational changes of SecD would be communicated to the outer membrane.
405

406 **HTL interacts with the periplasmic chaperone SurA in complex with OmpA**

407 The results above lead us to address outstanding questions regarding chaperone interaction
408 with the Sec complex. When proteins emerge from the channel into the periplasm they are
409 presumably quickly engaged by chaperones, prime examples being Skp and SurA (McMorran
410 et al., 2013; Sklar et al., 2007). So far, no evidence has been presented of a direct interaction of
411 these chaperones with the Sec-machinery. As noted above, the core SecYEG complex does not
412 contain periplasmic domains large enough to do so. We explored the possibility of such an
413 interaction with the HTL, using the same approach described above for HTL variants and BAM
414 (Fig. 2a, Fig. S4a).

415 Addition of SurA to the HTL (without cross-linking) followed by glycerol gradient
416 centrifugation yielded heavy fractions containing HTL and SurA (Fig. S11a), indicative of them
417 being in complex. As in the case for the HTL-BAM binding experiment, only low yields of the
418 HTL-SurA complex were generated. Again, this is understandable because of the likely
419 transient nature of the translocon-chaperone interaction. To overcome this the experiment was
420 repeated in the presence of cross-linker (Grafix) and fractions were prepared for NS-EM (Fig.
421 S11b).

422 The subsequent analysis revealed a structure with dimensions of roughly 300 x 250 x 150
423 Å, large enough to contain both HTL and SurA (Fig. 6a). To overcome the uncertainty, due to
424 the low yield of HTL-SurA recovery, we decided to verify the presence and location of SurA
425 on the isolated complex. To do so, the complex was immuno-decorated with a polyclonal
426 antibody raised against SurA (Fig. 6b. Fig. S11c-d) or, as a control, a monoclonal antibody
427 specific to a cytosolic loop of SecY (Corey et al., 2016) (Fig. 6c, Fig. S11e-f). The results mark
428 the location of the cytosolic face of SecY (Fig. 6c), and SurA as a prominent extention on the
429 other periplasmic side of the inner-membrane closest to SecDF-YidC.

430 The experiment was repeated using SurA purified in complex with a classical OMP
431 substrate, OmpA (Fig. 6d,e; Fig. S12a-b). The NS-EM structure of HTL-SurA-OmpA shows
432 additional density compared to HTL-SurA, roughly adjacent to the channel exit site of SecYEG
433 and in contact with SurA, possibly representing a late inner-membrane translocation
434 intermediate (Fig. 7).
435
436
437 **DISCUSSION**
438 The *in vivo* and *in vitro* analyses described here demonstrate a direct, functional interaction
439 between the Sec and BAM translocons, mediated by the extended periplasmic domains
440 possessed by BAM (Ma et al., 2019), SecDF (Furukawa et al., 2017) and YidC (Kumazaki et
441 al., 2014), but not SecYEG. Evidently, direct contact between HTL and BAM is required for
442 efficient OMP biogenesis in rapidly growing cells. The interaction could enable large protein
443 fluxes to stream through the periplasm, while minimising aggregation and proteolysis (Fig. 7).
444 The presence of a super-complex that bridges both membranes appears to be a fundamental
445 feature of the Gram negative bacterial cell envelope, the importance of which is only just
446 coming to the fore (Rassam et al., 2015; 2018).
447 It has already been shown that the HTL contains a lipid-containing cavity within the
448 membrane, presumably to facilitate membrane protein insertion (Botte et al., 2016; Martin et
449 al., 2019). Remarkably, in the super-complex between HTL and BAM there is a much larger
450 extension of this cavity opening into the periplasm (Fig. 2). This would seem an obvious place
451 for OMP passage and for the interaction with chaperones, and is of sufficient size to do so (Fig.
452 7). The cavity is situated such that secretory protein could enter *via* the protein-channel through
453 SecYEG, and then exit accordingly into the periplasm or into the mouth of the BAM complex.
454 It remains to be seen how the Sec-BAM complex and the periplasmic chaperones coordinate.
455 Perhaps these chaperones recognise emerging protein at the Sec-machinery and shuttle them
456 into the periplasm, with or without the need for the BAM complex. Otherwise, they could
457 facilitate the passage through the inter-membrane assembly for OM folding and insertion (Fig.
458 7). We show the interaction of SurA, as well as an OMP-SurA complex, with HTL;
459 incriminating at least this chaperone with the early stages of transport through the cell wall, *i.e.*
460 immediately after precursor cleavage. Furthermore, SurA is known to interact with BamA

461 (Sklar et al., 2007), suggesting its involvement throughout OMP passage from the Sec to BAM
462 (Fig. 7).
463 Other ancillary factors of the Sec machinery have also been implicated: YfgM and PpiD are
464 thought to mediate interactions with periplasmic chaperones (Götzke et al., 2014), the latter of
465 which has also been shown to interact with SecYEG and YidC (Jauß et al., 2019). Interestingly,
466 *yfgL* and *yfgM* are in the same operon (Blattner et al., 1997); the former encoding a subunit of
467 the BAM complex (BamB) (Wu et al., 2005). Indeed, a recent proteomic analysis of the *E. coli*
468 'membrane protein interactome' identifies cross-membrane interactions involving SecYEG,
469 BAM and the chaperones YfgM and PpiD (Carlson et al., 2019). Understanding the interplay
470 of various periplasmic chaperones during OMP passage through the Sec-BAM assembly to the
471 outer membrane will require further attention.
472 From our data it is clear that the periplasmic domain of SecD is central to the physical BAM-
473 HTL interaction. Even more intriguing though is the requirement for a functioning proton wire
474 through the SecDF trans-membrane domain. This raises the intriguing prospect of a TonB-style
475 energy-coupling from the inner membrane (Celia et al., 2016): *i.e.* the transmission of free
476 energy available from ATP turnover and the PMF from the Sec-machinery (Arkowitz and
477 Wickner, 1994; Brundage et al., 1990; Schiebel et al., 1991), for OMP folding and insertion at
478 the outer-membrane. We therefore propose that one of the primary roles of SecDF is in inter-
479 membrane trafficking and chemiosmotic energy transduction. Indeed, we and others have
480 shown that ATP- and PMF-driven transport of proteins through the inner membrane is
481 dependent only on SecYEG and SecA (Brundage et al., 1990; Schulze et al., 2014); while we
482 show here proton translocation through SecD is crucial for efficient OMP folding and growth.
483 Thus, there appears to be two distinct requirements of the PMF in protein secretion: one for
484 the early stage – SecA driven translocation through SecYEG at the inner membrane, and
485 another for late stages of OMP maturation. The latter could be facilitated by conformational
486 changes in SecDF, for transduction of energy from the inner to the outer membrane. When a
487 key proton carrying residue of the inner membrane segment of the translocon is neutralised –
488 $SecD_{D519N}$ – the conformation of the periplasmic domain is perturbed (Furukawa et al., 2017).
489 Presumably then, successive protonation (approximated by $SecD_{D519N}$) and deprotonation result
490 in large, long-range, cyclical conformational changes during PMF driven proton transport from
491 the periplasm to the cytosol. Interestingly, the phospholipid cardiolipin (CL) is also important

492 for the association of the Sec and BAM machineries; it is probably not a coincidence that this
493 lipid has already been shown to be critical for PMF driven protein translocation through
494 SecYEG (Corey et al., 2018).
495 Taking all together, this builds a compelling case for SecD mediated inter-membrane energy
496 transduction for outer membrane protein folding and insertion – in keeping with other members
497 of the RND transporter family, such as the assembly of AcrAB (inner membrane) and TolC
498 (outer membrane) (Du et al., 2014; Wang et al., 2017). Direct association between inner and
499 outer membrane components appears to be the rule rather than the exception for transporters
500 embedded in double membrane systems: parallels with the translocation assembly module
501 (TAM) for auto-transporter secretion (Selkrig et al., 2012) and the TIC-TOC import machinery
502 of chloroplasts (Chen et al., 2018) are particularly striking, given the respective outer-
503 membrane components (TamA and TOC75) are homologous of BamA. Particularly intriguing
504 is the possibility of the mitochondrial homologue of BAM (Sorting and Assembly Machinery;
505 SAM) participating in analogous inter-membrane interactions between respective inner and
506 outer membranes. Indeed, subunits of the MItochondrial contact site and Cristae Organizing
507 System (MICOS) connect the energy-transducing ATP synthase of the inner membrane and
508 SAM at the outer-membrane (Ott et al., 2015; Rampelt et al., 2017).
509
510

511 **MATERIALS AND METHODS**

512

513 **Strains and plasmids**

514 *E. coli* C43 (DE3) was a gift from Sir John Walker (MRC Mitochondrial Biology Unit,
515 Cambridge, UK) (Miroux and Walker, 1996). *E. coli* BL21 (DE3) were purchased as competent
516 cells (New England Biolabs). *E. coli ΔsecG* (KN425 (W3110 M25 *ΔsecG*::kan)) (Nishiyama et
517 al., 1994), which lacks a genomic copy of *secG*, was obtained from Prof. Frank Duong (University
518 of British Colombia, Vancouver, Canada). *E. coli* strain JP352 (Kan^r), which contains an
519 arabinose-regulated *secDF-yajC* operon (Economou et al., 1995), was given to us by Prof. Ross
520 Dalbey.

521 The plasmids for over-expression of *secEYG* and *yidC* were from our laboratory collection
522 (Collinson et al., 2001; Lotz et al., 2008), the former and also that of *secDF* were acquired from
523 Prof. Frank Duong (Duong and Wickner, 1997). Vectors designed for over-production of HTL,
524 HTL(ΔYidC) and HTL($SecD_{D519N}$) were created using the ACEMBL expression system
525 (Bieniossek et al., 2009; Botte et al., 2016). The vector for *bamABCDE* over-expression pJH114
526 (Amp^r) was a gift from Prof. Harris Bernstein (Roman-Hernandez et al., 2014); from which
527 pJH114-*bamACDE* (ΔBamB) was produced by linear PCR with primers designed to flank the
528 BamB gene and amplify DNA around it. FseI restriction sites were included in the primers to ligate
529 the amplified DNA. pBAD-SecDF(ΔP1) was generated by amplifying SecDF(ΔP1) from pBAD-
530 SecDF and cloning it between the pBAD NcoI and HindIII sites. pET28b-*surA* and pET11a-*ompA*
531 (Schiffrin et al., 2017) were gifts from Prof. Sheena Radford (The Astbury Centre for Structural
532 Molecular Biology, University of Leeds, UK).
533 For SecDF depletion experiments, SecDF was cloned into pTrc99a (Amp^r, IPTG-inducible),
534 and the $secD_{D519N}$ mutation was subsequently made by changing the WT carrying plasmid using a
535 site-directed ligase-independent PCR method.
536
537 **SDS-PAGE, western blotting and antibodies**
538 All SDS-PAGE was performed with either *Invitrogen* Bolt 4-12% Bis-Tris gels or *Invitrogen*
539 midi 4-12% Bis-Tris gels. For western blotting, proteins were transferred onto nitrocellulose
540 membrane. Mouse monoclonal antibodies against SecY, SecE and SecG were from our laboratory
541 collection (used at 1:10000 dilution). Polyclonal antibodies against SecD and BamA were
542 generated commercially in rabbits, and SecA in sheep from purified proteins (All used at 1:5000
543 dilution). BamB and BamD antibodies were gifts from Dr Harris Bertstein (1:5000 dilution). The
544 SurA antibody was purchased from 2BScientific (1:10000 dilution). A secondary antibody
545 conjugated to DyLight800 was used for SecG and SecY (Thermo Fisher Scientific, 1:10000
546 dilution), whereas a HRP-conjugated secondary antibody was used for SecD and BamA (1:10000
547 dilution).
548
549 **Protein production and purification**
550 HTL, HTL(ΔYidC), HTL($SecD_{D519N}$), SecYEG, YidC, SecDF and SurA were purified as
551 described previously (Burmann et al., 2013; Collinson et al., 2001; Lotz et al., 2008; Schulze et

552 al., 2014). BAM and BAM(ΔBamB) was over-produced in *E. coli* C43 according to established
553 protocols (Iadanza et al., 2016; Roman-Hernandez et al., 2014). For preparation of SurA and SurA-
554 OmpA complexes, both proteins were over-produced separately in 1 L of cultures as described
555 previously (Humes et al., 2019). Both were harvested by centrifugation, lysed in a cell disruptor
556 (Constant Systems Ltd.) and resuspended in 20 mL 20 mM Tris pH 8.0, 130 mM NaCl, 10% (v/v)
557 glycerol ($TS_{130}G$) in the presence of cOmplete protein inhibitor cocktail (Roche). The resulting
558 samples were clarified by centrifugation in an SS34 rotor (27,000 x*g*, 4°C, 20 minutes, Sorvall).
559 For OmpA, the supernatant was discarded and the pellet resuspended in 20 mL $TS_{130}G$ + 6 M urea.
560 The OmpA pellet was diluted to 80 mL with 6 M urea and mixed with the SurA supernant to give
561 a final urea concentration of 4.8 M. The urea was removed by dialysing in 2 L $TS_{130}G$ for 6 hours
562 at room temperature, then dialysing overnight at 4°C in 5 L fresh $TS_{130}G$. The sample was
563 centrifuged under the same conditions as above and the supernatant loaded onto a 5 mL HisTrap
564 HP column equilibrated with $TS_{50}G$. The column was washed with $TS_{50}G$ + 20 mM imidazole,
565 and bound proteins eluted with $TS_{50}G$ + 300 mM imidazole. The eluents were loaded onto a HiTrap
566 Q HP column equilibrated in $TS_{50}G$ and free SurA was found in the unbound fraction. A linear
567 gradient of 0.05 - 1 M NaCl was applied over 60 mL and the fractions containing SurA-OmpA
568 were taken for further analyses.
569
570 **Isolation of inner and outer membranes**
571 1 L of *E. coli* cultures over-producing SecYEG, HTL, SecDF or SecDF(ΔP1) were produced as
572 described previously (Collinson et al., 2001; Komar et al., 2016; Schulze et al., 2014). The
573 harvested cell pellets were resuspended in 20 mL $TS_{130}G$, homogenised with a potter, passed twice
574 through a cell disruptor (Constant Systems Ltd.) for lysis and centrifuged to remove debris (SS34
575 rotor, Sorvall, 12,000 x*g*, 20 minutes, 4°C). The supernatant was taken and layered upon 20 mL
576 $TS_{130}G$ + 20% (w/v) sucrose in a Ti45 tube and centrifuged (Ti45 rotor, Beckmann-Coulter,
577 167,000 x*g*, 120 minutes, 4°C). The pellet was taken, resuspended in 4 mL $TS_{130}G$, homogenised
578 with a potter and layered upon a sucrose gradient prepared in an SW32 centrifuge tube composed
579 of 5 mL layers of $TS_{130}G$ + 55% (w/v), 48%, 41%, 34% and 28% sucrose. The sample was then
580 fractionated by centrifugation (SW32 rotor, Beckmann-Coulter, 130,000 x*g*, 15 hours, 4°C). Upon
581 completion, the light to heavy fractions were analysed by SDS PAGE and western blotting.
582

583 **Co-immunoprecipitations (co-IPs) with *E. coli* total membrane extracts**

584 Membrane pellets of *E. coli* strains C43 (WT), C43 pJH114-*bamABCDE* (Amp^r), *ΔsecG* (Kan^r),
585 WT *lpp*, mutant lpp_{+21} and JP325 (containing variants of pTrc as specified in text, cultures grown
586 in glucose for depletion of endogenous SecDFyajC), were prepared as described previously
587 (Collinson et al., 2001), with *bamABCDE* over-expression achieved as before (Roman-Hernandez
588 et al., 2014). The pellets were resuspended in $TS_{130}G$ to 120 mg/mL, homogenised and solubilised
589 with 0.5% DDM for 1 hour at 4°C. The solubilised material was clarified by ultra-centrifugation
590 (160,000 x*g* for 45 mins) and the membrane extracts were analysed.

591 For co-IPs pulling on SecG antibody, 250 uL of protein G resin was washed in a spin column
592 with 200 mM NaCl, 20 mM HEPES pH 8.0 (HS buffer), and blocked overnight in HS buffer + 2%
593 (w/v) BSA at 4°C. Meanwhile, 7.5 µL of purified SecG monoclonal antibody was added to 500
594 µL of the membrane extracts and incubated overnight at 4°C. The following morning, the resin
595 was washed thoroughly in HS buffer containing either 0.02% (w/v) DDM or 0.02% (w/v) DDM
596 with 0.002% (w/v) CL, resuspended back to 250 µL and added to the 500 µL of membrane extract
597 for three hours rotating gently at room temperature. The resin was separated from the extracts by
598 centrifugation in a spin column at 2,000 x*g* for 1 minute, washed 7 times with 350 µL HS buffer,
599 followed by one final wash with 150 µL HS buffer, which was collected in a fresh tube for analysis
600 (to which 50 uL of 4x LDS sample buffer was added once collected). The bound material was then
601 eluted by addition of 150 uL 1 x LDS sample buffer (to which an additional 50 uL of 1x LDS
602 sample buffer was added once collected). Samples were analysed by SDS PAGE and western
603 blotting.

604 For co-affinity adsorption by pulling on the hexa-histidine tag of recombinant BamA, 100 µL
605 of nickel-charged chelating resin was added to 500 µL of membrane extracts and incubated for 5
606 minutes at room temperature. The resin was then separated from the extract and treated in the same
607 way as described above but with $TS_{130}G$ + 0.02% (w/v) DDM/ 0.002% (w/v) CL + 30 mM
608 imidazole (washing) or 300 mM imidazole (elution).

609 Statistical analyses were conducted using GraphPad Prism. An unpaired T-test was used to
610 compare pull down samples (p value = 0.05, * = < 0.05, ** = < 0.01, *** = < 0.001, specific p
611 values are stated in figure legends).

612

613 ***In vitro* assembly and purification of complexes for EM and XL-MS**

614 All protein complexes visualized by negative stain EM were formed by incubating 5 µM of the
615 respective proteins in binding buffer (20 mM HEPES pH 8.0, 250 mM NaCl, 0.03% (w/v) DDM/
616 0.003% (w/v) CL) at 30ºC for 30 minutes with shaking in a total volume of 150 µl. The protein
617 complexes were purified in a glycerol/ glutaraldehyde gradient (20 - 40% (w/v) and 0 - 0.15%
618 (w/v), respectively) by centrifugation at 34,000 RPM in a SW60 Ti rotor (Beckmann-Coulter) for
619 16 hours at 4ºC. Mobility controls of individual and partial complexes (BAM, and HTL) or
620 individual proteins (SecYEG, YidC, SecDF, SurA) without the glutaraldehyde gradient were
621 performed under the same conditions. Gradients were fractionated in 150 µl aliquots and those
622 with glutaraldehyde were inactivated with 50 mM of Tris pH 8.0. Aliquots were analysed by SDS-
623 PAGE and silver staining. For HTL:SurA:Ab_{SurA} and Ab_{SecY}:HTL:SurA complexes, 5 µM of HTL
624 and SurA were incubated in binding buffer at 30ºC for 30 minutes with shaking in a total volume
625 of 150 µl. Antibodies were added at concentrations of 1 in 7.5 or 1 in 15 for the SecY or SurA
626 antibodies respectively, these were incubated at 30ºC for 15 minutes before complex purification
627 as described above.
628 The HTL:BAM complex for cryoEM was formed by incubating 8 µM of the HTL and BAM
629 complexes in binding buffer (50 mM HEPES pH 8.0, 200 mM NaCl, 0.01% (w/v) DDM / 0.001%
630 (w/v) CL at 30ºC for 20 minutes with shaking in a total volume of 250 µl. After 20 min, 0.05% of
631 glutaraldehyde was added to the sample and incubated for 10 minutes at 21ºC. The crosslinker was
632 inactivated with 30 mM Tris pH 8.0 and the sample was loaded onto a Superose 6 Increase 10/300
633 GL (GE healthcare) column equilibrated in GF buffer (30 mM Tris pH 8.0, 200 mM NaCl, 0.01%
634 (w/v) DDM). Fractions were analysed by SDS-PAGE and silver staining.
635 The HTL:BAM complex for cross-linked mass spectroscopy (XL-MS) analysis was prepared
636 following the same procedure described for the cryo-EM preparation, but the sample was
637 crosslinked with 1.5 mM DSBU and inactivated with 20 mM of ammonium carbonate pH 8.0
638 before loaded onto the gel filtration column.
639
640 **XL-MS analysis**
641 The DSBU cross-linked HTL:BAM complex was precipitated by methanol and chloroform
642 (Wessel and Flügge, 1984) and the pellet dissolved in 8 M urea. After reduction with 10 mM DTT
643 (one hour at 37ºC) and alkylation with 50 mM iodoacetamide (30 minutes in the dark at RT), the
644 sample was diluted 1:5 with 62.5 mM ammonium hydrogen carbonate and digested with trypsin

645 (1:20 w/w) overnight at 37ºC. Digestion was stopped by the addition of formic acid to a final
646 concentration of 2% (v/v) and the sample split in two equal amounts for fractionation by size
647 exclusion (SEC) and reverse phase C18 at high pH chromatography. A Superdex Peptide 3.2/300
648 column (GE Healthcare) was used for SEC fractionation by isocratic elution with 30% (v/v)
649 acetonitrile/ 0.1% (v/v) TFA at a flow rate of 50 µL/ min. Fractions were collected every minute
650 from 1.0 mL to 1.7 mL of elution volume. Reverse phase C18 high pH fractionation was carried
651 out on an Acquity UPLC CSH C18 1.7 µm, 1.0 x 100 mm column (Waters) over a gradient of
652 acetonitrile 2-40% (v/v) and ammonium hydrogen bicarbonate 100 mM.
653 All the fractions were lyophilized and resuspended in 2% (v/v) acetonitrile and 2% (v/v) formic
654 acid for LC–MS/MS analysis. An Ultimate U3000 HPLC (ThermoScientific Dionex, USA) was
655 used to deliver a flow of approximately 300 nL/ min. A C18 Acclaim PepMap100 5 µm,
656 100 µm × 20 mm nanoViper (ThermoScientific Dionex, USA), trapped the peptides before
657 separation on a C18 Acclaim PepMap100 3 µm, 75 µm × 250 mm nanoViper (ThermoScientific
658 Dionex, USA). Peptides were eluted with a gradient of acetonitrile. The analytical column was
659 directly interfaced *via* a nano-flow electrospray ionisation source, with a hybrid quadrupole
660 orbitrap mass spectrometer (Q-Exactive HF-X, ThermoScientific, USA). MS data were acquired
661 in data-dependent mode. High-resolution full scans (R=120,000, m/z 350-2000) were recorded in
662 the Orbitrap and after CID activation (stepped collision energy 30 ± 3) of the 10 most intense MS
663 peaks, MS/ MS scans (R=45,000) were acquired.
664 For data analysis, Xcalibur raw files were converted into the MGF format through MSConvert
665 (Proteowizard (Kessner et al., 2008)) and used directly as input files for MeroX (Götze et al.,
666 2015). Searches were performed against an ad-hoc protein database containing the sequences of
667 the complexes and a set of randomised decoy sequences generated by the software. The following
668 parameters were set for the searches: maximum number of missed cleavages 3; targeted residues
669 K; minimum peptide length 5 amino acids; variable modifications: carbamidomethyl-Cys (mass
670 shift 57.02146 Da), Met-oxidation (mass shift 15.99491 Da); DSBU modification fragments:
671 85.05276 Da and 111.03203 (precision: 5 ppm MS (Kessner et al., 2008) and 10 ppm MS (Götze
672 et al., 2015)); False Discovery Rate cut-off: 5%. Finally, each fragmentation spectra were manually
673 inspected and validated.
674
675

676 **EM and image processing**

677 For negative stain, aliquots of sucrose gradient fractions containing the different complexes
678 were applied to glow-discharged (15 s) carbon grids with Cu 300 mesh, washed and stained with
679 2% (w/ v) uranyl acetate (1 min). Digital images were acquired with two different microscopes; a
680 Tecnai 12 with a Ceta 16M camera (ThermoFisher Scientific) at a digital magnification of 49,000
681 x and a sampling resolution of 2.04 Å per pixel, and in a Tecnai 12 with a Gatan Camera One View
682 at a digital magnification of 59,400 and a sampling resolution of 2.1 Å per pixel. Image processing
683 was performed using the EM software framework Scipion v1.2 (la Rosa-Trevín et al., 2016).
684 Several thousand particles were manually and semi-automatic supervised selected as input for
685 automatic particle picking through the XMIPP3 package (Abrishami et al., 2013; la Rosa-Trevín
686 et al., 2013). Particles were then extracted with the Relion v2.1 package (Kimanius et al., 2016;
687 Scheres, 2012a) and classified with a free-pattern maximum-likelihood method (Relion 2D-
688 classification). After manually removing low quality 2D classes, a second round of 2D
689 classification was performed with Relion and XMIPP-CL2D in parallel (Sorzano et al., 2010).
690 Representative 2D averages were used to generate several initial 3D models with the EMAN v2.12
691 software (Scheres, 2012b; Tang et al., 2007). Extensive rounds of 3D classification were then
692 carried out using Relion 3D-classification due to the heterogeneity of the sample. The most
693 consistent models were used for subsequent 3D classifications. For the final 3D volume
694 refinement, Relion auto-refine or XMIPP3-Projection Matching were used. Resolution was
695 estimated with Fourier shell correlation using 0.143 correlation coefficient criteria (Rosenthal and
696 Henderson, 2003; Scheres and Chen, 2012). See Table S2 for image processing details.

697 For CryoEM, appropriate fractions of the glutaraldehyde-crosslinked HTL:BAM complex
698 purified by gel filtration were applied to glow-discharged (20 s) Quantifoil grids (R1.2/R1.3, Cu
699 300 mesh) with an ultrathin carbon layer (2 nm), blotted and plunged into a liquid ethane chamber
700 in a Leica EM. Two data sets from the same grid were acquired in a FEI Talos Arctica cryo-
701 electron microscope operated at 200 kV and equipped with a K2 detector at calibrated
702 magnification of 79000 x. The first data set with 2056 images recorded, had a 1.75 Å/px sample
703 resolution, dose rate of 2.26 electrons/Å^2 and 20 s exposure time fractionated in 40 frames. Defocus
704 values oscillated between -1.5 nm and -3.0 nm. The second data set with 3703 images recorded,
705 had a 0.875 Å/px sample resolution, dose rate of 2.47 electrons/Å^2 and 18 s exposure time
706 fractionated in 40 frames. Defocus values oscillated between – 1.0 nm and -2.2 nm. Particles were

707 picked in the same way as for negative stain, and were binned to a 1.75 Å/px sample resolution
708 before merging to the first data set. Image processing was performed using the EM software
709 framework Scipion v1.2 (la Rosa-Trevín et al., 2016) with a similar strategy of the NS-EM samples
710 but also using extensive masking procedures (Fig. S6).
711 All 3D reconstructions were calculated using a home-built workstation (CPU Intel Core i7
712 7820X, 2x Asus Turbo GTX 1080Ti, 16Gb RAM DDR4) and partial usage of HPC clusters
713 (Bluecrystal 4 and Bluecryo) at the University of Bristol.
714
715
716 **Depletion of SecDF-YajC**
717 *E. coli* strain JP352 was transformed with an empty pTrc99a, or the same plasmid, but cloned
718 with either WT *secDF* or s*ecD*$_{D519N}$*F*. Precultures of the strains were prepared in 100 mL 2xYT
719 media supplemented with 0.2% (w/v) arabinose, ampicillin (for pTrc selectivity) and kanamycin
720 (for JP352 selectivity). The following morning, the cells were harvested by centrifugation and
721 resuspended with 50 mL fresh 2xYT (no arabinose). This washing procedure was repeated two
722 more times to remove excess arabinose. Prewarmed (37ºC) 1 L 2xYT cultures containing either
723 0.2% (w/v) arabinose or 0.5% (w/v) glucose were then inoculated with the preculture such that a
724 final $OD_{600\ nm}$ of 0.05 was achieved. An aliquot was taken every 1.5 hours for 6 hours. Induction
725 of pTrc with IPTG was not necessary as background expression was sufficient to achieve levels of
726 SecD similar to that of JP325 cultured in the presence of arabinose. Periplasmic and outer
727 membrane fractions were produced by preparing spheroplasts (Birdsell and Cota-Robles, 1967),
728 centrifuging the samples at 12000 x*g* for 5 minutes, taking the supernatant (a mixture of
729 periplasmic and OM fractions) and removing the OM fraction by ultracentrifugation at 160000 x*g*
730 for 20 minutes. The fractions were then subjected to SDS-PAGE and western blotting.
731
732 **Measurement of protein transport**
733 Inner membrane vesicles (IMVs) were produced from BL21(DE3) cells overproducing HTL,
734 HTL(SecD$_{D519N}$), SecYEG or with empty pBAD as described previously (Corey et al., 2018).
735 Transport experiments with and without PMF were performed in triplicate using established
736 methods (Corey et al., 2018).
737

Acknowledgments

We are particularly grateful for the generosity of Dr Harris Bernstein for the kind gifts of the *bamABCDE* expression construct (pJH114) and antibodies, and Prof. Sheena Radford for *surA* and *ompA* expression plasmids. Thanks to Prof. Daniel Daley for telling us about YfgL and YfgM. We thank Dr Remy Martin for brewing, and for making the HTL $secD_{D519N}F$ mutant. We acknowledge access and support of the Wolfson Bioimaging Facility and the GW4 Facility for High-Resolution Electron Cryo-Microscopy, with particular thanks to Dr Ufuk Borucu. We are grateful to Mr Tom Batstone for the support at the computer cluster BlueCryo.

Funding: This work was funded by the BBSRC (BB/S008349/1 to IC, DWW and SA; BB/N015126/1 to IC and DWW; BB/M003604/1 to IC and SA; SWBioDTP – BB/J014400/1 and BB/J014400/1 to LT), EMBO (Long Term Fellowship – ALTF 710-2015, LTFCOFUND2013 and GA-2013-609409 – to SA) and the Elizabeth Blackwell Institute for Health Research, University of Bristol (Elizabeth Blackwell Bridging fellowship to SA). The GW4 Facility for High-Resolution Electron Cryo-Microscopy was funded by the Wellcome Trust (electron microscope with direct electron detector; 202904/Z/16/Z and 206181/Z/17/Z) and BBSRC (computer cluster; BB/R000484/1).

Author contribution: SA, DWW, LT, WA and IC designed and conducted experiments, assisted by JL; SA, DWW, LT and IC wrote the manuscript; VAMG and BD provided facilities and expertise, and edited the manuscript; EJC and MB, helped with the Lpp experiments – conception, strain provision and text editing; GD and JMS, conducted the XL-MS experiments, processed the data, helped in their description and interpretation; IC, VAMG, BD and MB secured funding; IC led the project.

Declaration: the authors declare no competing interests.

766 **Data and materials availability:** All data are available in the main text or the supplementary
767 materials. The HTL-BAM cryo-EM structure has been deposited at the EMDB under the
768 accession number 11240.

769

770 **REFERENCES**

771

772 Abrishami, V., Zaldívar-Peraza, A., la Rosa-Trevín, de, J.M., Vargas, J., Otón, J., Marabini, R.,
773 Shkolnisky, Y., Carazo, J.M., and Sorzano, C.O.S. (2013). A pattern matching approach to the
774 automatic selection of particles from low-contrast electron micrographs. Bioinformatics *29*,
775 2460–2468.

776 Arkowitz, R.A., and Wickner, W. (1994). SecD and SecF are required for the proton
777 electrochemical gradient stimulation of preprotein translocation. Embo J. *13*, 954–963.

778 Asmar, A.T., Ferreira, J.L., Cohen, E.J., Cho, S.-H., Beeby, M., Hughes, K.T., and Collet, J.-F.
779 (2017). Communication across the bacterial cell envelope depends on the size of the periplasm.
780 PLoS Biol. *15*, e2004303.

781 Bakelar, J., Buchanan, S.K., and Noinaj, N. (2016). The structure of the β-barrel assembly
782 machinery complex. Science *351*, 180–186.

783 Bieniossek, C., Nie, Y., Frey, D., Olieric, N., Schaffitzel, C., Collinson, I., Romier, C., Berger,
784 P., Richmond, T.J., Steinmetz, M.O., et al. (2009). Automated unrestricted multigene
785 recombineering for multiprotein complex production. Nat. Methods *6*, 447–450.

786 Birdsell, D.C., and Cota-Robles, E.H. (1967). Production and ultrastructure of lysozyme and
787 ethylenediaminetetraacetate-lysozyme spheroplasts of Escherichia coli. J. Bacteriol. *93*, 427–
788 437.

789 Blattner, F.R., Plunkett, G., Bloch, C.A., Perna, N.T., Burland, V., Riley, M., Collado-Vides, J.,
790 Glasner, J.D., Rode, C.K., Mayhew, G.F., et al. (1997). The complete genome sequence of
791 Escherichia coli K-12. Science *277*, 1453–1462.

792 Botte, M., Zaccai, N.R., Nijeholt, J.L.À., Martin, R., Knoops, K., Papai, G., Zou, J., Deniaud, A.,
793 Karuppasamy, M., Jiang, Q., et al. (2016). A central cavity within the holo-translocon suggests a
794 mechanism for membrane protein insertion. Sci Rep *6*, 38399.

795 Brundage, L., Hendrick, J.P., Schiebel, E., Driessen, A.J., and Wickner, W. (1990). The purified
796 E. coli integral membrane protein SecY/E is sufficient for reconstitution of SecA-dependent
797 precursor protein translocation. Cell *62*, 649–657.

798 Bulieris, P.V., Behrens, S., Holst, O., and Kleinschmidt, J.H. (2003). Folding and insertion of the
799 outer membrane protein OmpA is assisted by the chaperone Skp and by lipopolysaccharide. J.
800 Biol. Chem. *278*, 9092–9099.

801 Burmann, B.M., Wang, C., and Hiller, S. (2013). Conformation and dynamics of the periplasmic
802 membrane-protein-chaperone complexes OmpX-Skp and tOmpA-Skp. Nat. Struct. Mol. Biol.
803 *20*, 1265–1272.

804 Carlson, M.L., Stacey, R.G., Young, J.W., Wason, I.S., Zhao, Z., Rattray, D.G., Scott, N., Kerr,
805 C.H., Babu, M., Foster, L.J., et al. (2019). Profiling the Escherichia coli membrane protein
806 interactome captured in Peptidisc libraries. eLife *8*.

807 Celia, H., Noinaj, N., Zakharov, S.D., Bordignon, E., Botos, I., Santamaria, M., Barnard, T.J.,
808 Cramer, W.A., Lloubes, R., and Buchanan, S.K. (2016). Structural insight into the role of the
809 Ton complex in energy transduction. Nature *538*, 60–65.

810 Chang, C.N., Blobel, G., and Model, P. (1978). Detection of prokaryotic signal peptidase in an
811 Escherichia coli membrane fraction: endoproteolytic cleavage of nascent f1 pre-coat protein.
812 Proc. Natl. Acad. Sci. U.S.a. *75*, 361–365.

813 Chen, Y.-L., Chen, L.-J., Chu, C.-C., Huang, P.-K., Wen, J.-R., and Li, H.-M. (2018). TIC236
814 links the outer and inner membrane translocons of the chloroplast. Nature.

815 Chorev, D.S., Baker, L.A., Wu, D., Beilsten-Edmands, V., Rouse, S.L., Zeev-Ben-Mordehai, T.,
816 Jiko, C., Samsudin, F., Gerle, C., Khalid, S., et al. (2018). Protein assemblies ejected directly
817 from native membranes yield complexes for mass spectrometry. Science *362*, 829–834.

818 Cohen, E.J., Ferreira, J.L., Ladinsky, M.S., Beeby, M., and Hughes, K.T. (2017). Nanoscale-
819 length control of the flagellar driveshaft requires hitting the tethered outer membrane. Science
820 *356*, 197–200.

821 Collinson, I., Breyton, C., Duong, F., Tziatzios, C., Schubert, D., Or, E., Rapoport, T., and
822 Kühlbrandt, W. (2001). Projection structure and oligomeric properties of a bacterial core protein
823 translocase. Embo J. *20*, 2462–2471.

824 Collinson, I. (2019). The Dynamic ATP-Driven Mechanism of Bacterial Protein Translocation
825 and the Critical Role of Phospholipids. Front Microbiol *10*, 1217.

826 Corey, R.A., Allen, W.J., Komar, J., Masiulis, S., Menzies, S., Robson, A., and Collinson, I.
827 (2016). Unlocking the Bacterial SecY Translocon. Structure *24*, 518–527.

828 Corey, R.A., Pyle, E., Allen, W.J., Watkins, D.W., Casiraghi, M., Miroux, B., Arechaga, I.,
829 Politis, A., and Collinson, I. (2018). Specific cardiolipin-SecY interactions are required for
830 proton-motive force stimulation of protein secretion. Proc. Natl. Acad. Sci. U.S.a. *115*, 7967–
831 7972.

832 Cranford-Smith, T., and Huber, D. (2018). The way is the goal: how SecA transports proteins
833 across the cytoplasmic membrane in bacteria. FEMS Microbiol. Lett. *365*.

834 Du, D., Wang, Z., James, N.R., Voss, J.E., Klimont, E., Ohene-Agyei, T., Venter, H., Chiu, W.,
835 and Luisi, B.F. (2014). Structure of the AcrAB-TolC multidrug efflux pump. Nature *509*, 512–
836 515.

837 Duong, F., and Wickner, W. (1997). Distinct catalytic roles of the SecYE, SecG and SecDFyajC
838 subunits of preprotein translocase holoenzyme. Embo J. *16*, 2756–2768.

839 Economou, A., Pogliano, J.A., Beckwith, J., Oliver, D.B., and Wickner, W. (1995). SecA
840 membrane cycling at SecYEG is driven by distinct ATP binding and hydrolysis events and is
841 regulated by SecD and SecF. Cell *83*, 1171–1181.

842 Eicher, T., Seeger, M.A., Anselmi, C., Zhou, W., Brandstätter, L., Verrey, F., Diederichs, K.,
843 Faraldo-Gómez, J.D., and Pos, K.M. (2014). Coupling of remote alternating-access transport
844 mechanisms for protons and substrates in the multidrug efflux pump AcrB. eLife *3*.

845 Furukawa, A., Nakayama, S., Yoshikaie, K., Tanaka, Y., and Tsukazaki, T. (2018). Remote
846 Coupled Drastic β-Barrel to β-Sheet Transition of the Protein Translocation Motor. Structure *26*,
847 485–489.e2.

848 Furukawa, A., Yoshikaie, K., Mori, T., Mori, H., Morimoto, Y.V., Sugano, Y., Iwaki, S.,
849 Minamino, T., Sugita, Y., Tanaka, Y., et al. (2017). Tunnel Formation Inferred from the I-Form
850 Structures of the Proton-Driven Protein Secretion Motor SecDF. Cell Rep *19*, 895–901.

851 Gardel, C., Benson, S., Hunt, J., Michaelis, S., and Beckwith, J. (1987). secD, a new gene
852 involved in protein export in Escherichia coli. J. Bacteriol. *169*, 1286–1290.

853 Gold, V.A.M., Robson, A., Bao, H., Romantsov, T., Duong, F., and Collinson, I. (2010). The
854 action of cardiolipin on the bacterial translocon. Proc. Natl. Acad. Sci. U.S.a. *107*, 10044–10049.

855 Götze, M., Pettelkau, J., Fritzsche, R., Ihling, C.H., Schäfer, M., and Sinz, A. (2015). Automated
856 assignment of MS/MS cleavable cross-links in protein 3D-structure analysis. J. Am. Soc. Mass
857 Spectrom. *26*, 83–97.

858 Götzke, H., Palombo, I., Muheim, C., Perrody, E., Genevaux, P., Kudva, R., Muller, M., and
859 Daley, D.O. (2014). YfgM is an ancillary subunit of the SecYEG translocon in Escherichia coli.
860 J. Biol. Chem. *289*, 19089–19097.

861 Green, E.R., and Mecsas, J. (2016). Bacterial Secretion Systems: An Overview. Microbiol Spectr
862 *4*.

863 Gu, Y., Li, H., Dong, H., Zeng, Y., Zhang, Z., Paterson, N.G., Stansfeld, P.J., Wang, Z., Zhang,
864 Y., Wang, W., et al. (2016). Structural basis of outer membrane protein insertion by the BAM
865 complex. Nature *531*, 64–69.

866 Hendrick, J.P., and Wickner, W. (1991). SecA protein needs both acidic phospholipids and
867 SecY/E protein for functional high-affinity binding to the Escherichia coli plasma membrane. J.
868 Biol. Chem. *266*, 24596–24600.

869 Humes, J.R., Schiffrin, B., Calabrese, A.N., Higgins, A.J., Westhead, D.R., Brockwell, D.J., and
870 Radford, S.E. (2019). The Role of SurA PPIase Domains in Preventing Aggregation of the
871 Outer-Membrane Proteins tOmpA and OmpT. J. Mol. Biol.

872 Iadanza, M.G., Higgins, A.J., Schiffrin, B., Calabrese, A.N., Brockwell, D.J., Ashcroft, A.E.,
873 Radford, S.E., and Ranson, N.A. (2016). Lateral opening in the intact β-barrel assembly
874 machinery captured by cryo-EM. Nature Communications *7*, 12865.

875 Jauß, B., Petriman, N.A., Drepper, F., Franz, L., Sachelaru, I., Welte, T., Steinberg, R.,
876 Warscheid, B., and Koch, H.-G. (2019). Non-competitive binding of PpiD and YidC to the
877 SecYEG translocon expands the global view on the SecYEG interactome in E. coli. J. Biol.
878 Chem.

879 Josefsson, L.G., and Randall, L.L. (1981). Different exported proteins in E. coli show differences
880 in the temporal mode of processing in vivo. Cell *25*, 151–157.

881 Kastner, B., Fischer, N., Golas, M.M., Sander, B., Dube, P., Boehringer, D., Hartmuth, K.,
882 Deckert, J., Hauer, F., Wolf, E., et al. (2008). GraFix: sample preparation for single-particle
883 electron cryomicroscopy. Nat. Methods *5*, 53–55.

884 Kessner, D., Chambers, M., Burke, R., Agus, D., and Mallick, P. (2008). ProteoWizard: open
885 source software for rapid proteomics tools development. Bioinformatics *24*, 2534–2536.

886 Kimanius, D., Forsberg, B.O., Scheres, S.H., and Lindahl, E. (2016). Accelerated cryo-EM
887 structure determination with parallelisation using GPUs in RELION-2. eLife *5*.

888 Komar, J., Alvira, S., Schulze, R.J., Martin, R., Lycklama A Nijeholt, J.A., Lee, S.C., Dafforn,
889 T.R., Deckers-Hebestreit, G., Berger, I., Schaffitzel, C., et al. (2016). Membrane protein
890 insertion and assembly by the bacterial holo-translocon SecYEG-SecDF-YajC-YidC. Biochem.
891 J. *473*, 3341–3354.

892 Konovalova, A., Kahne, D.E., and Silhavy, T.J. (2017). Outer Membrane Biogenesis. Annu.
893 Rev. Microbiol. *71*, 539–556.

894 Kumazaki, K., Kumazaki, K., Kishimoto, T., Kishimoto, T., Furukawa, A., Furukawa, A., Mori,
895 H., Mori, H., Tanaka, Y., Tanaka, Y., et al. (2014). Crystal structure of Escherichia coli YidC, a
896 membrane protein chaperone and insertase. Sci Rep *4*, 7299.

897 la Rosa-Trevín, de, J.M., Otón, J., Marabini, R., Zaldívar, A., Vargas, J., Carazo, J.M., and
898 Sorzano, C.O.S. (2013). Xmipp 3.0: an improved software suite for image processing in electron
899 microscopy. J. Struct. Biol. *184*, 321–328.

900 la Rosa-Trevín, de, J.M., Quintana, A., Del Cano, L., Zaldívar, A., Foche, I., Gutiérrez, J.,
901 Gómez-Blanco, J., Burguet-Castell, J., Cuenca-Alba, J., Abrishami, V., et al. (2016). Scipion: A
902 software framework toward integration, reproducibility and validation in 3D electron
903 microscopy. J. Struct. Biol. *195*, 93–99.

904 Lill, R., Cunningham, K., Brundage, L.A., Ito, K., Oliver, D., and Wickner, W. (1989). SecA
905 protein hydrolyzes ATP and is an essential component of the protein translocation ATPase of
906 Escherichia coli. Embo J. *8*, 961–966.

907 Lotz, M., Haase, W., Kühlbrandt, W., and Collinson, I. (2008). Projection structure of yidC: a

908 conserved mediator of membrane protein assembly. J. Mol. Biol. *375*, 901–907.

909 Ma, X., Wang, Q., Li, Y., Tan, P., Wu, H., Wang, P., Dong, X., Hong, L., and Meng, G. (2019).
910 How BamA recruits OMP substrates via poly-POTRAs domain. Faseb J. fj201900681RR.

911 Martin, R., Larsen, A.H., Corey, R.A., Midtgaard, S.R., Frielinghaus, H., Schaffitzel, C., Arleth,
912 L., and Collinson, I. (2019). Structure and Dynamics of the Central Lipid Pool and Proteins of
913 the Bacterial Holo-Translocon. Biophys. J.

914 McMorran, L.M., Bartlett, A.I., Huysmans, G.H.M., Radford, S.E., and Brockwell, D.J. (2013).
915 Dissecting the effects of periplasmic chaperones on the in vitro folding of the outer membrane
916 protein PagP. J. Mol. Biol. *425*, 3178–3191.

917 Mio, K., Tsukazaki, T., Mori, H., Kawata, M., Moriya, T., Sasaki, Y., Ishitani, R., Ito, K.,
918 Nureki, O., and Sato, C. (2014). Conformational variation of the translocon enhancing chaperone
919 SecDF. J. Struct. Funct. Genomics *15*, 107–115.

920 Miroux, B., and Walker, J.E. (1996). Over-production of proteins in Escherichia coli: mutant
921 hosts that allow synthesis of some membrane proteins and globular proteins at high levels. J.
922 Mol. Biol. *260*, 289–298.

923 Nishiyama, K., Hanada, M., and Tokuda, H. (1994). Disruption of the gene encoding p12 (SecG)
924 reveals the direct involvement and important function of SecG in the protein translocation of
925 Escherichia coli at low temperature. Embo J. *13*, 3272–3277.

926 Nouwen, N., and Driessen, A.J.M. (2002). SecDFyajC forms a heterotetrameric complex with
927 YidC. Mol. Microbiol. *44*, 1397–1405.

928 Ott, C., Dorsch, E., Fraunholz, M., Straub, S., and Kozjak-Pavlovic, V. (2015). Detailed analysis
929 of the human mitochondrial contact site complex indicate a hierarchy of subunits. PLoS ONE *10*,
930 e0120213.

931 Pogliano, J.A., and Beckwith, J. (1994). SecD and SecF facilitate protein export in Escherichia
932 coli. Embo J. *13*, 554–561.

933 Rampelt, H., Bohnert, M., Zerbes, R.M., Horvath, S.E., Warscheid, B., Pfanner, N., and van der
934 Laan, M. (2017). Mic10, a Core Subunit of the Mitochondrial Contact Site and Cristae
935 Organizing System, Interacts with the Dimeric F1Fo-ATP Synthase. J. Mol. Biol. *429*, 1162–
936 1170.

937 Rassam, P., Copeland, N.A., Birkholz, O., Tóth, C., Chavent, M., Duncan, A.L., Cross, S.J.,
938 Housden, N.G., Kaminska, R., Seger, U., et al. (2015). Supramolecular assemblies underpin
939 turnover of outer membrane proteins in bacteria. Nature *523*, 333–336.

940 Rassam, P., Long, K.R., Kaminska, R., Williams, D.J., Papadakos, G., Baumann, C.G., and
941 Kleanthous, C. (2018). Intermembrane crosstalk drives inner-membrane protein organization in
942 Escherichia coli. Nature Communications *9*, 1082.

943 Ricci, D.P., and Silhavy, T.J. (2019). Outer Membrane Protein Insertion by the β-barrel
944 Assembly Machine. EcoSal Plus *8*.

945 Roman-Hernandez, G., Peterson, J.H., and Bernstein, H.D. (2014). Reconstitution of bacterial
946 autotransporter assembly using purified components. eLife *3*, e04234.

947 Rosenthal, P.B., and Henderson, R. (2003). Optimal determination of particle orientation,
948 absolute hand, and contrast loss in single-particle electron cryomicroscopy. J. Mol. Biol. *333*,
949 721–745.

950 Samuelson, J.C., Chen, M., Jiang, F., Möller, I., Wiedmann, M., Kuhn, A., Phillips, G.J., and
951 Dalbey, R.E. (2000). YidC mediates membrane protein insertion in bacteria. Nature *406*, 637–
952 641.

953 Scheres, S.H.W. (2012a). RELION: implementation of a Bayesian approach to cryo-EM
954 structure determination. J. Struct. Biol. *180*, 519–530.

955 Scheres, S.H.W. (2012b). A Bayesian view on cryo-EM structure determination. J. Mol. Biol.
956 *415*, 406–418.

957 Scheres, S.H.W., and Chen, S. (2012). Prevention of overfitting in cryo-EM structure
958 determination. Nat. Methods *9*, 853–854.

959 Schiebel, E., Driessen, A.J., Hartl, F.U., and Wickner, W. (1991). Delta mu H+ and ATP
960 function at different steps of the catalytic cycle of preprotein translocase. Cell *64*, 927–939.

961 Schiffrin, B., Calabrese, A.N., Higgins, A.J., Humes, J.R., Ashcroft, A.E., Kalli, A.C.,
962 Brockwell, D.J., and Radford, S.E. (2017). Effects of Periplasmic Chaperones and Membrane
963 Thickness on BamA-Catalyzed Outer-Membrane Protein Folding. J. Mol. Biol. *429*, 3776–3792.

964 Schulze, R.J., Komar, J., Botte, M., Allen, W.J., Whitehouse, S., Gold, V.A.M., Lycklama A
965 Nijeholt, J.A., Huard, K., Berger, I., Schaffitzel, C., et al. (2014). Membrane protein insertion
966 and proton-motive-force-dependent secretion through the bacterial holo-translocon SecYEG-
967 SecDF-YajC-YidC. Proc. Natl. Acad. Sci. U.S.a. *111*, 4844–4849.

968 Scotti, P.A., Urbanus, M.L., Brunner, J., de Gier, J.W., Heijne, von, G., van der Does, C.,
969 Driessen, A.J., Oudega, B., and Luirink, J. (2000). YidC, the Escherichia coli homologue of
970 mitochondrial Oxa1p, is a component of the Sec translocase. Embo J. *19*, 542–549.

971 Selkrig, J., Mosbahi, K., Webb, C.T., Belousoff, M.J., Perry, A.J., Wells, T.J., Morris, F.,
972 Leyton, D.L., Totsika, M., Phan, M.-D., et al. (2012). Discovery of an archetypal protein
973 transport system in bacterial outer membranes. Nat. Struct. Mol. Biol. *19*, 506–10–S1.

974 Sklar, J.G., Wu, T., Kahne, D., and Silhavy, T.J. (2007). Defining the roles of the periplasmic
975 chaperones SurA, Skp, and DegP in Escherichia coli. Genes Dev. *21*, 2473–2484.

976 Sorzano, C.O.S., Bilbao-Castro, J.R., Shkolnisky, Y., Alcorlo, M., Melero, R., Caffarena-
977 Fernández, G., Li, M., Xu, G., Marabini, R., and Carazo, J.M. (2010). A clustering approach to

978 multireference alignment of single-particle projections in electron microscopy. J. Struct. Biol.
979 *171*, 197–206.

980 Tang, G., Peng, L., Baldwin, P.R., Mann, D.S., Jiang, W., Rees, I., and Ludtke, S.J. (2007).
981 EMAN2: an extensible image processing suite for electron microscopy. J. Struct. Biol. *157*, 38–
982 46.

983 Tseng, T.T., Gratwick, K.S., Kollman, J., Park, D., Nies, D.H., Goffeau, A., and Saier, M.H.
984 (1999). The RND permease superfamily: an ancient, ubiquitous and diverse family that includes
985 human disease and development proteins. J. Mol. Microbiol. Biotechnol. *1*, 107–125.

986 Van den Berg, B., Clemons, W.M., Collinson, I., Modis, Y., Hartmann, E., Harrison, S.C., and
987 Rapoport, T.A. (2004). X-ray structure of a protein-conducting channel. Nature *427*, 36–44.

988 Voulhoux, R., Bos, M.P., Geurtsen, J., Mols, M., and Tommassen, J. (2003). Role of a highly
989 conserved bacterial protein in outer membrane protein assembly. Science *299*, 262–265.

990 Wang, Z., Fan, G., Hryc, C.F., Blaza, J.N., Serysheva, I.I., Schmid, M.F., Chiu, W., Luisi, B.F.,
991 and Du, D. (2017). An allosteric transport mechanism for the AcrAB-TolC multidrug efflux
992 pump. eLife *6*.

993 Wessel, D., and Flügge, U.I. (1984). A method for the quantitative recovery of protein in dilute
994 solution in the presence of detergents and lipids. Anal. Biochem. *138*, 141–143.

995 Wu, T., Malinverni, J., Ruiz, N., Kim, S., Silhavy, T.J., and Kahne, D. (2005). Identification of a
996 multicomponent complex required for outer membrane biogenesis in Escherichia coli. Cell *121*,
997 235–245.

998 Zuber, B., Chami, M., Houssin, C., Dubochet, J., Griffiths, G., and Daffé, M. (2008). Direct
999 visualization of the outer membrane of mycobacteria and corynebacteria in their native state. J.
1000 Bacteriol. *190*, 5672–5680.

1001

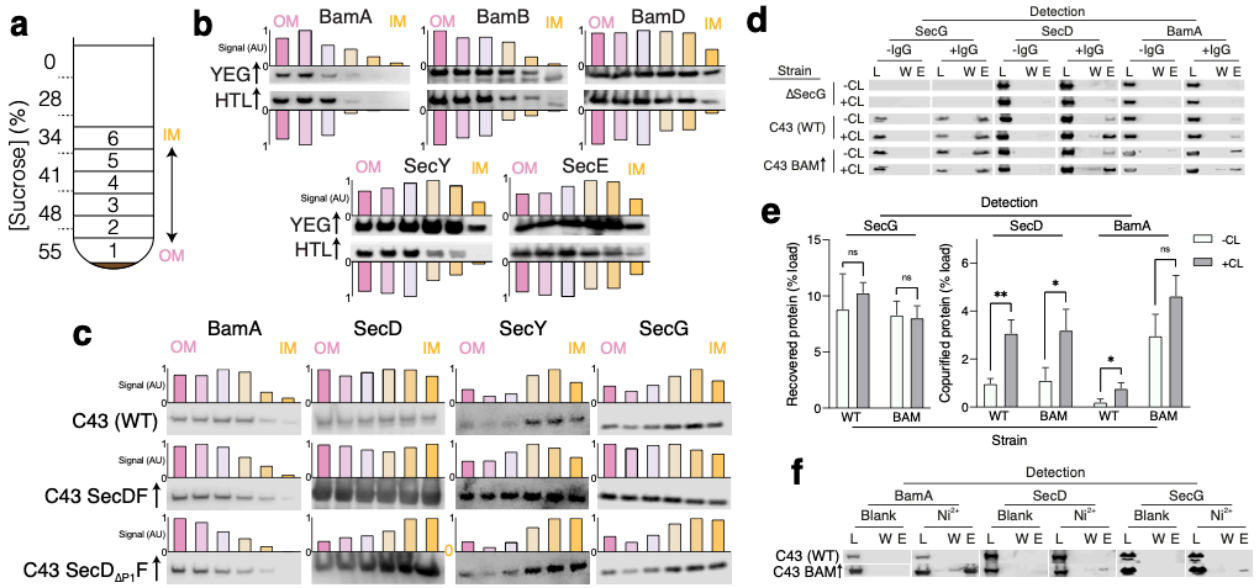
a
[Sucrose] (%)
0
28
34
41
48
55
6
5
4
3
2
1
IM
OM
b
BamA
BamB
BamD
SecY
SecE
OM
IM
Signal (AU)
YEG
HTL
c
BamA
SecD
SecY
SecG
C43 (WT)
C43 SecDF
C43 SecD$_{\Delta P1}$F
d
Detection
SecG
SecD
BamA
-IgG
+IgG
Strain
ΔSecG
C43 (WT)
C43 BAM
-CL
+CL
L
W
E
e
Recovered protein (% load)
Copurified protein (% load)
WT
BAM
Strain
ns
**
*
f
Blank
Ni^{2+}
C43 (WT)
C43 BAM

1023 **Figure. 1: Identification of interactions between HTL and BAM**

1024

1025 **a.** Schematic representation of sucrose gradient centrifugation tube for fractionation of *E. coli*
1026 total membranes. Numbers 1-6 indicate the fractions taken for SDS PAGE and immunoblotting
1027 shown in **b, c** and **d**.
1028
1029 **b, c.** Immunoblots of fractions produced as shown in **a** for membranes of *E. coli* C43
1030 overproducing either SecYEG or HTL (**b**) or for *E. coli* C43 with no over-expression, and those
1031 over-producing either SecDF or $SecD_{\Delta P1}F$ (lacking the periplasmic domain 1 (P1) of SecD) (**c**).
1032 To help visualise migration shifts, blotting signal was used to quantify relative abundances of
1033 proteins of interest, shown above or below blots as normalised bar charts.
1034
1035 **d.** Co-immuno-precipitations (co-IP) of SecG, SecD and BamA – pulling with the SecG
1036 antibody. Pull-downs were conducted with solubilised crude membrane extracts from *E. coli*
1037 C43 (WT), a strain lacking SecG (Δ*secG*), and C43 over-producing BAM. Experiments were
1038 conducted in the presence (+CL) and absence (-CL) of cardiolipin. L = load (1% total material),
1039 W = final wash before elution (to demonstrate proper washing of affinity resin, 17% of total
1040 material) and E = elution (17% of total material).
1041
1042 **e.** Quantification of IPs shown in (**d**). Error bars represent SEM. An unpaired T-test was used
1043 to compare samples ($p = 0.05$, $n = 3$, * = < 0.05, ** = < 0.01, p values from left to right are
1044 0.4874, 0.8083, 0.0041, 0.0249, 0.0241 and 0.0839).
1045
1046 **f.** Affinity pull-down of recombinant $BamA\text{-}His_6$, SecD and SecG by nickel chelation all in the
1047 presence of cardiolipin. L, W and E as described in **(d).**

1048

1049

1050

1051

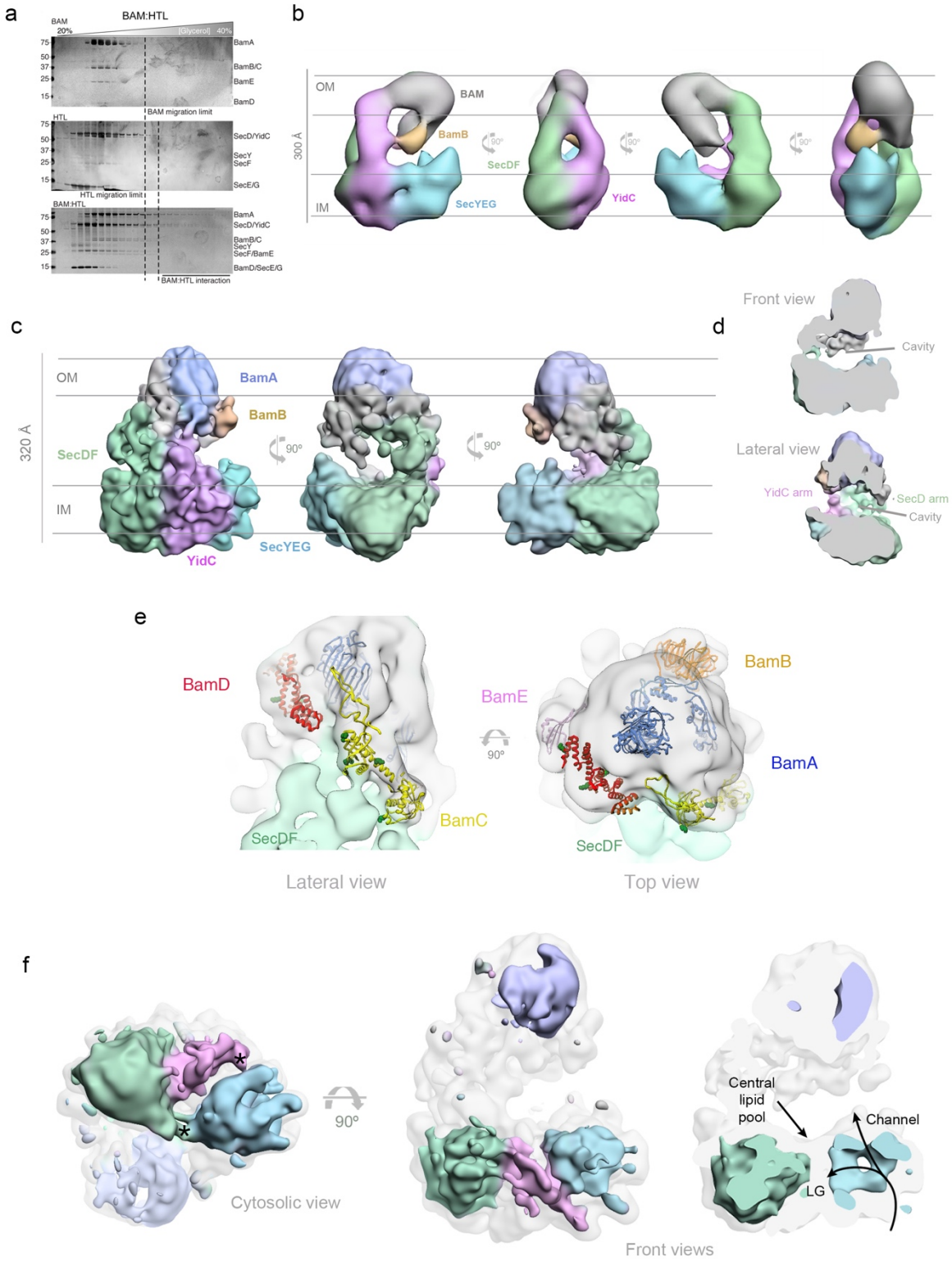

1052

1053

1054

1055 **Figure. 2: 3D characterization of HTL-BAM by NS-EM and cryo-EM in detergent**
1056 **solution, and XL-MS analysis**

1057 **a**. Silver-stained SDS-PAGE gels of fractions from glycerol centrifugation gradients are shown,
1058 with increasingly large complexes appearing in fractions of higher percentage glycerol, (from left
1059 to right). The glycerol centrifugation gradients of BAM alone (top) HTL alone (middle) and HTL
1060 mixed with BAM (bottom) are shown. Dashed lines represent the fraction of furthest migration of
1061 the individual components, as determined in the top two gels.

1062 **b**. Negative stain analysis of the HTL-BAM complex (37.2 Å resolution) in four representative
1063 orthogonal views, with the orientation with respect to the inner and outer membranes inferred.
1064 BAM (grey), BamB (orange), SecYEG (cyan), YidC (pink) and SecDF (green) are shown.
1065
1066 **c**. Three orthogonal views of the cryo-EM HTL-BAM complex 3D reconstruction (27 Å
1067 resolution). Colours are as in (**a**), but with BamA in blue.
1068
1069 **d.** Frontal and lateral sliced views of the cryo HTL-BAM complex showing the large cavity
1070 between the IM and OM complexes.
1071
1072 **e.** Close-up of the outer-membrane region of the HTL-BAM complex. The cryo-EM structure
1073 (transparent surface) with BamABCDE atomic structures docked (pdb_5d0q). BamB (orange)
1074 position was determined directly by NS-EM (Fig. S4e). BamA (blue), BamC (yellow), BamD (red)
1075 and BamE (pink) are docked according to the HTL-BAM cryo-EM density and XLMS data (Fig.
1076 S6c). Green sphere atoms in BamC and BamD show interacting points with SecD identified by
1077 mass apectrometry.
1078
1079 **f**. Lower threshold map of HTL-BAM overlaid with the correct level (transparent grey), with
1080 the main components coloured as in (**a**). The lateral gate (LG) into the membrane, protein-
1081 channel through SecY and the central lipid pool are highlighted. The asterisks denote interaction
1082 sites between SecYEG and SecDF/ YidC.
1083
1084

1085

1086

1087

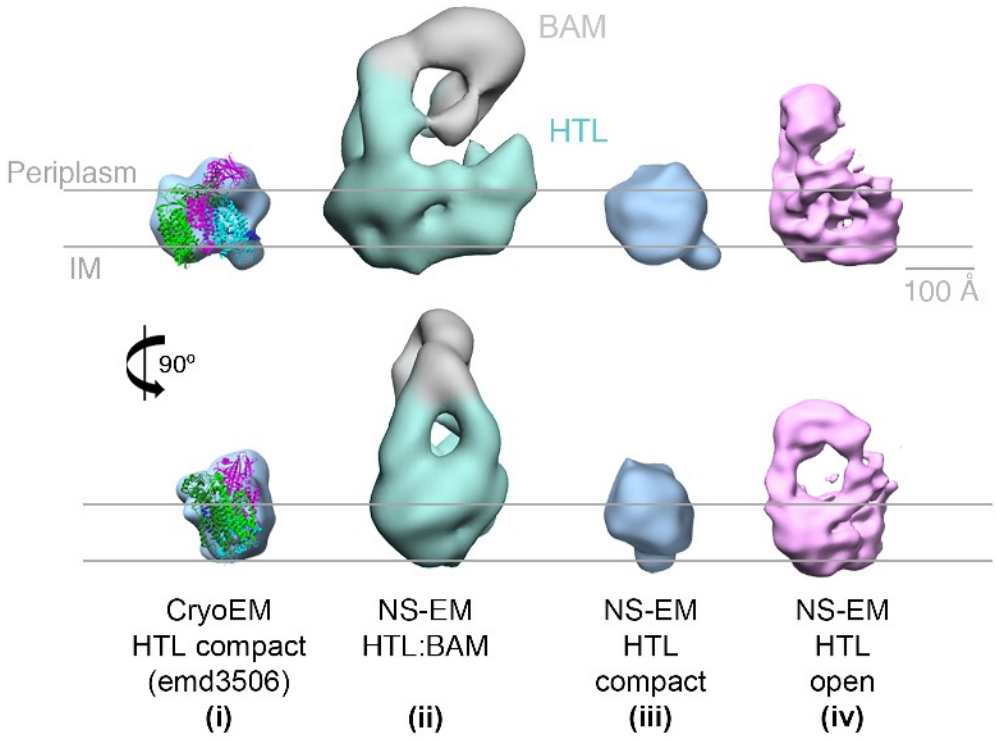

1088

1089

1090 **Figure 3: EM structures of HTL in 'compact' and 'open' states**

1091 Structure and docking of a previously published cryo-EM structure of HTL in the compact state
1092 **(i)** (Botte et al., 2016), the HTL-BAM complex **(ii)**, HTL in the 'compact' state **(iii)** and HTL
1093 in the 'open' state **(iv)**; structures **(ii - iv)** are from this study.

1094

1095

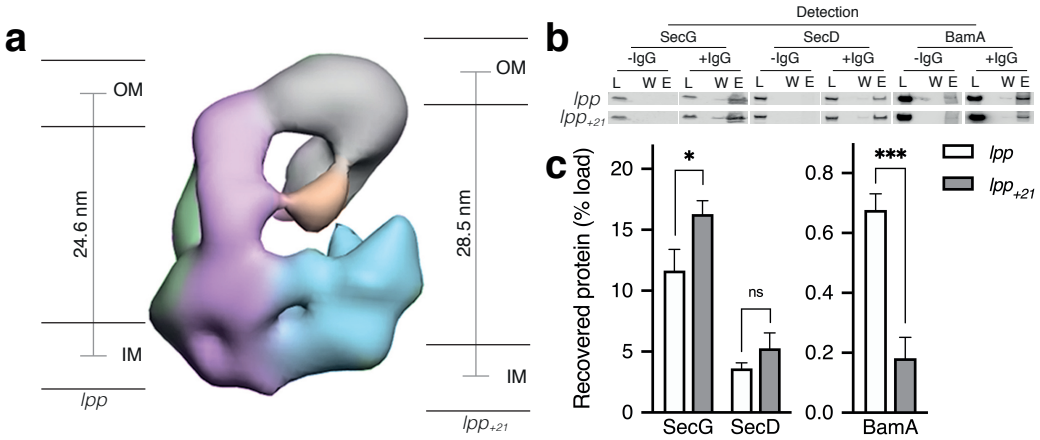

Figure 4: Effect of increasing the periplasmic distance on the HTL-BAM interaction

a. Negative-stain EM model of HTL-BAM (from Fig. 2a), annotated with membranes at the experimentally determined distances between the inner and outer membranes of *E. coli* strains containing wild type *lpp* and mutant lpp_{+21} (Asmar et al., 2017).

b. Co-immunoprecipitation of SecG, SecD and BamA when pulling from an anti-SecG monoclonal antibody. Co-IPs were conducted in the presence of cardiolipin as in Fig. 1d, but with solubilised membranes of strains described in **(a).**

c. Quantification of IPs from **(b)**. Error bars represent SEM. An unpaired T-test was used to compare samples ($p = 0.05$, $n = 3$, * = < 0.05, *** = < 0.001, p values from left to right are 0.0170, 0.0990 and 0.0006).

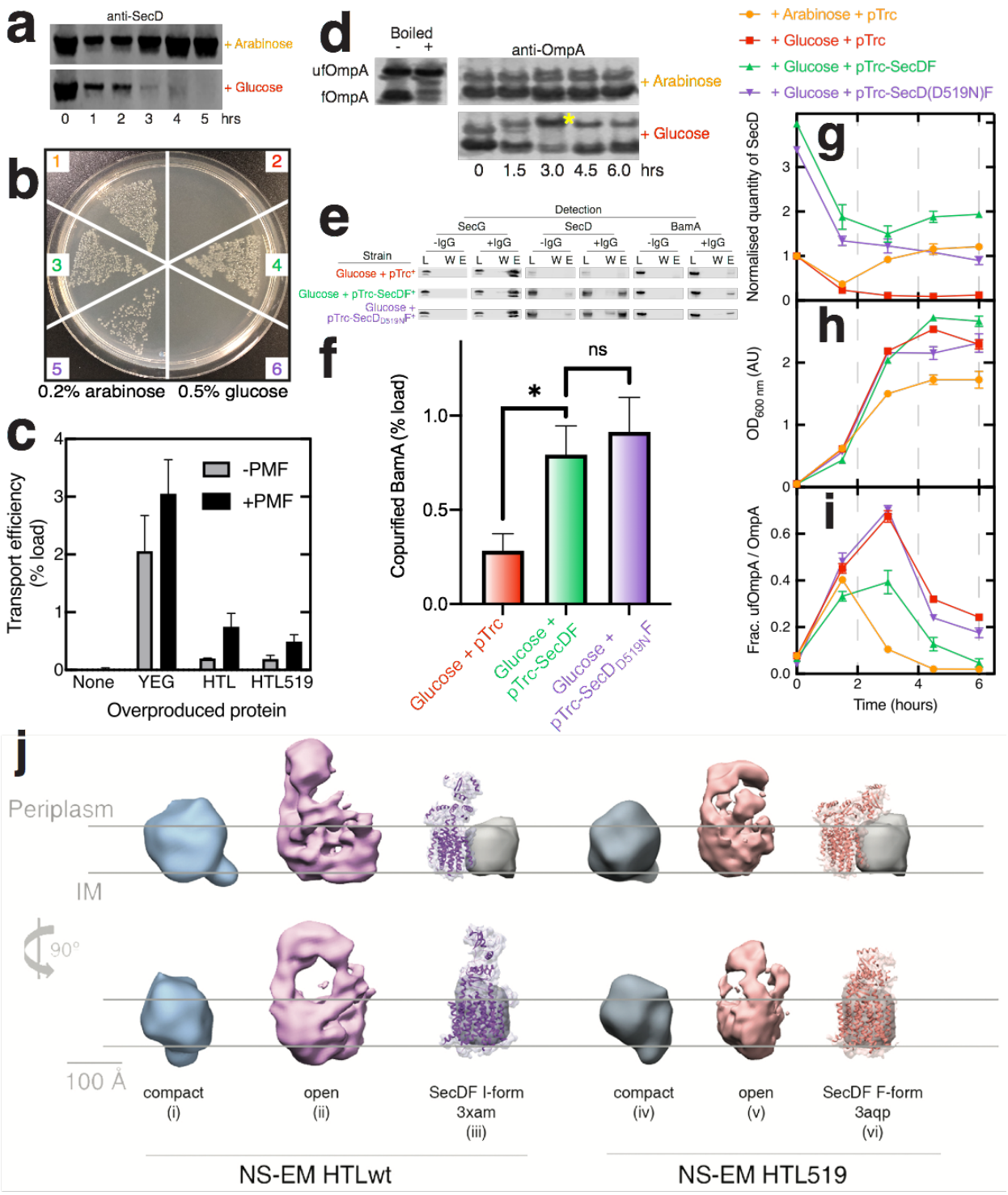

1112
1113
1114
1115
1116

1117 **Figure 5: Effects of SecD depletion upon cell growth, OmpA secretion and maturation**

1118

1119 **a**. Western blot illustrating depletion of SecD in *E. coli* JP325 whole cells when grown in the
1120 presence of arabinose or glucose. t=0 represents the time at which an overnight culture (grown
1121 in arabinose) was used to inoculate a fresh culture containing either arabinose or glucose.

1122

1123 **b.** Growth of *E. coli* JP325 transformed with empty vector pTrc99a (1 + 2), pTrc99a-*secDF* (3
1124 + 4) and pTrc99A-$secD_{D519N}F$ (5 + 6). Samples in panels 1, 3 and 5 were grown on LB-
1125 arabinose (permissive), whereas 2, 4 and 6 were grown on LB-glucose (non-permissive).

1126

1127 **c.** Classical SecA-driven import assay with *E. coli* inner membrane vesicles (IMVs) and OmpA.
1128 IMVs contained over-produced protein as stated on the x-axis. Error bars represent SEM (n=3).

1129

1130 **d.** Periplasmic fractions of *E. coli* JP325 immunoblotted for OmpA. Two species of OmpA are
1131 visible: folded OmpA (bottom band; fOmpA) and unfolded OmpA (top band; ufOmpA). Also
1132 shown are control lanes containing *E. coli* whole cells with over-produced, mainly 'folded'
1133 OmpA (fOmpA, bottom band) and the same sample, but boiled, to produce 'unfolded' OmpA
1134 (ufOmpA, top band).

1135

1136 **e.** Representative western blots of co-immuno-precipitations conducted as in Fig. 1d in the
1137 presence of CL, but with solubilised membranes prepared from *E. coli JP325* grown in the
1138 presence of glucose and cloned with variants of pTrc99a, as stated in the figure.

1139

1140 **f.** Quantification of BamA pull down from co-IPs shown in **(e)**. Error bars represent SEM. An
1141 unpaired T-test was used to compare samples ($p = 0.05$, $n = 3$, * = < 0.05, p values from left to
1142 right are 0.0449 and 0.6412).

1143

1144 For **(g-i)**, samples were prepared from various cell cultures; see key (above) for strains used.
1145 Error bars represent SEM (n=3 for experimental samples grown in glucose).

1146

1147 **g.** Quantification of SecD from western blots such as those shown in **(a)**. Values are normalised
1148 to JP325-pTrc99a at t = 0.
1149
1150 **h.** Culture growth curves.
1151
1152 **i.** Analysis of western blots such as those from **(d)** showing the quantity of ufOmpA as a fraction
1153 of the total OmpA in the periplasmic fraction.
1154
1155 **j**. Comparison of NS-EM structures of 'compact' (structures i and iv) and 'open' (structures ii
1156 and v) conformations of HTL *versus* the counterpart containing $SecD_{D519N}F$ (HTL519); both in
1157 the presence of CL. Atomic structures of SecDF overlaid with filtered maps at 5 Å are shown
1158 alongside for the *I*-form (structure iii, 3XAM) and *F*-form (structure vi, 3AQP), with the amino
1159 acid substitution equivalent to the *E.coli* $SecD_{D519N}$, 3AQP). The grey arbitrary mass indicates
1160 the approximate position and mass of SecYEG.
1161
1162
1163
1164

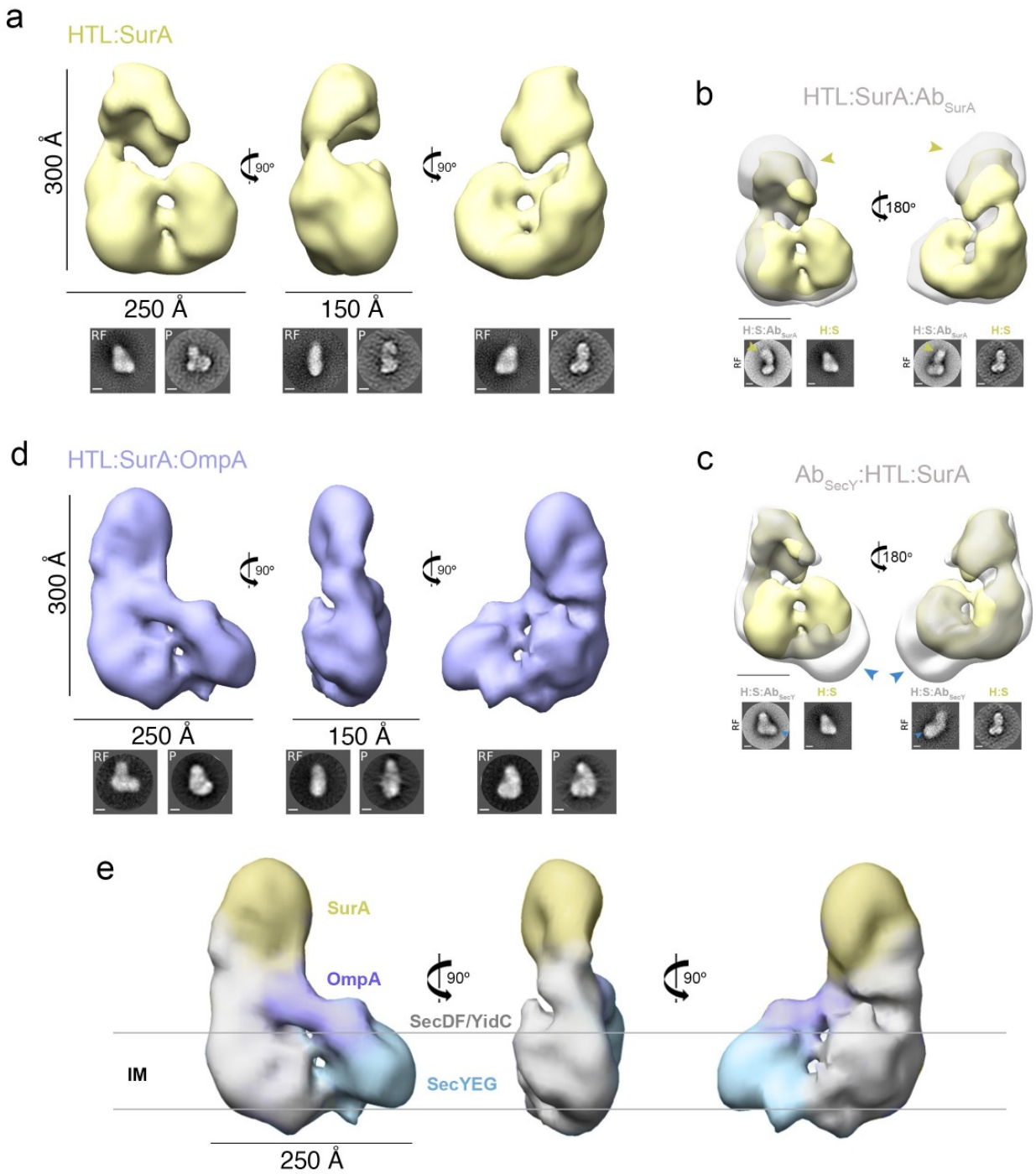

1165
1166
1167
1168
1169
1170

1171 **Figure. 6: Negative-stain analysis of HTL:SurA and HTL:SurA-OmpA complexes**

1172

1173 For **a**, **b, c** and **d** top panel shows views of 3D reconstructions, and bottom shows reference-
1174 free (RF) class averages and projections (P) of the final model, shown in the same orientations
1175 as the top. Scale bars are 100 Å, unless stated otherwise. See Table S2 for image processing
1176 details.

1177

1178 **a.** Orthogonal views of the HTL-SurA complex 3D reconstruction (41.9 Å resolution).

1179

1180 **b.** Opposing side views of the HTL-SurA complex (yellow) superimposed on the immuno-
1181 complex HTL-SurA:Ab_{SurA} complex (grey). The antibody (yellow arrows) is shown bound to
1182 the mass assigned to SurA.

1183

1184 **c.** Opposing side views of the HTL-SurA complex (yellow) superimposed on the immuno-
1185 complex Ab_{SecY}:HTL-SurA complex (grey). The antibody (blue arrows) is shown bound to the
1186 mass assigned to SecYEG.

1187

1188 **d.** Orthogonal side views of the HTL-SurA:OmpA complex 3D reconstruction (37.5 Å
1189 resolution).

1190

1191 **e**. Assigned map of the HTL-SurA-OmpA complex in the three representative orthogonal
1192 views, with components coloured accordingly.

1193

1194

1195

1196

1197

1198

1199

1200

1201

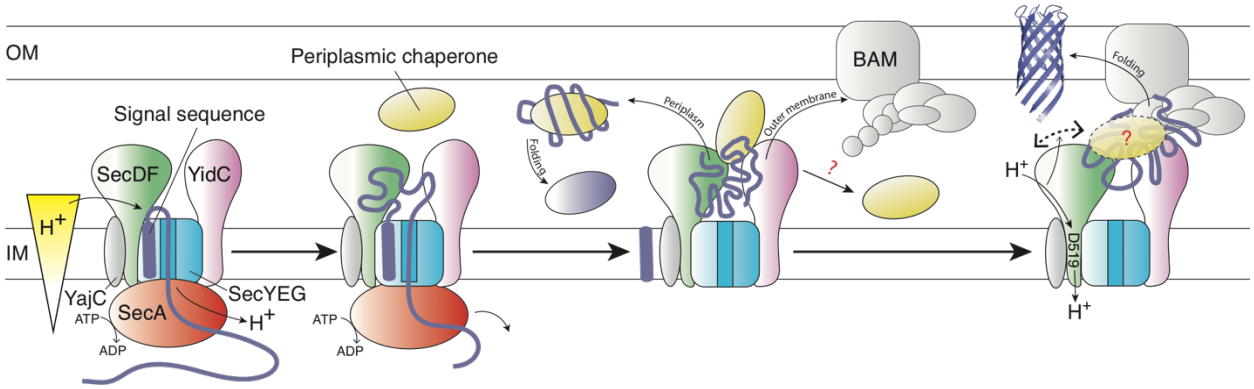

Figure 7: Schematic representation of the HTL:BAM machinery

Schematic model of OMP transfer through the bacterial envelope, facilitated by HTL-BAM and periplasmic chaperones, such as SurA, Skp, PpiD and YfgM. From left to right: OMP precursors with an N-terminal signal sequence are driven across the membrane by the ATPase SecA through the Sec translocon – the process is stimulated by PMF (independent of SecDF). Late in this process the pre-protein emerges into the periplasm and the signal sequence is removed, releasing the mature protein. Presumably, globular proteins are then guided into the periplasm, where folding will occur assisted by periplasmic chaperones. Otherwise, OMP-chaperone-HTL complexes are recognised by the BAM complex, with interactions forming between BAM and both HTL (this study) and SurA (Sklar et al., 2007). The persistence and variety of chaperones involvement at this stage is unclear (?). This conjunction enables the smooth and efficient passage of OMPs to the outer-membrane, enabled by energy coupling from the inner-membrane – trans-membrane proton-motive-force (PMF)-driven conformational changes *via* SecDF (right).

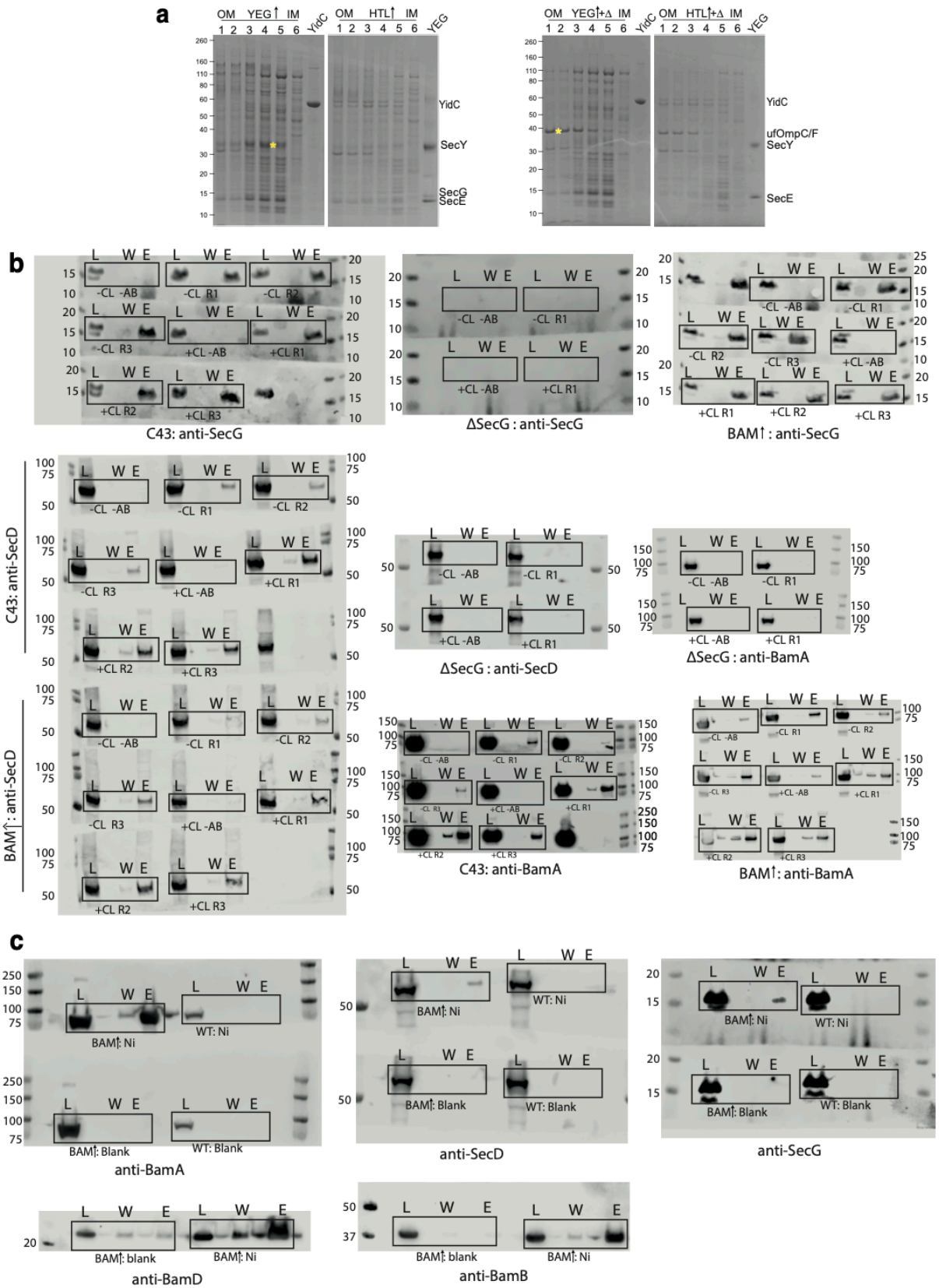
a
OM YEG↑ IM
1 2 3 4 5 6 YidC
OM HTL↑ IM
1 2 3 4 5 6 YEG
YidC
SecY
SecG
SecE
OM YEG↑+Δ IM
1 2 3 4 5 6 YidC
OM HTL↑+Δ IM
1 2 3 4 5 6 YEG
YidC
ufOmpC/F
SecY
SecE
b
C43: anti-SecG
ΔSecG : anti-SecG
BAM↑ : anti-SecG
C43: anti-SecD
BAM↑: anti-SecD
ΔSecG : anti-SecD
ΔSecG : anti-BamA
C43: anti-BamA
BAM↑: anti-BamA
c
BAM↑: Ni
WT: Ni
BAM↑: Blank
WT: Blank
anti-BamA
anti-SecD
anti-SecG
BAM↑: blank
anti-BamD
anti-BamB

1221

1222

1223
1224
1225 **Supplementary figure 1: Raw western blots of co-immuno-precipitations and affinity pull**
1226 **downs**
1227
1228 **a.** SDS PAGE stained for total protein of sucrose gradient fractions of *E. coli* C43 total
1229 membranes from cells over-producing SecYEG or HTL. Left and right gels show untreated and
1230 heat denatured (+Δ) samples respectively. Purified controls of SecYEG and YidC are also
1231 shown.
1232
1233 For (**b**) and (**c**), L = load (1% total material), W = final wash before elution (to demonstrate
1234 complete washing of affinity resin, 17% of total material) and E = elution (17% of total
1235 material).
1236
1237 **b.** Co-immunoprecipitations from Fig. 1d-e. Experiments were conducted in the presence
1238 (+CL) or absence (-CL) of augmented cardiolipin. Experiments were also carried out in the
1239 presence (+AB) or absence (-AB) of anti-SecG primary antibody, as a control to assess non-
1240 specific binding. Solubilised membranes of 3 cell strains were used: *E. coli* C43, a strain lacking
1241 SecG (Δ*secG*), and C43 over-producing BAM.
1242
1243 **c.** Affinity pull-downs from Fig. 1f. Experiments were conducted in with nickel-chelated (Ni)
1244 or non-chelated (blank) resin as a control to rule out non-specific binding.
1245
1246
1247
1248
1249
1250

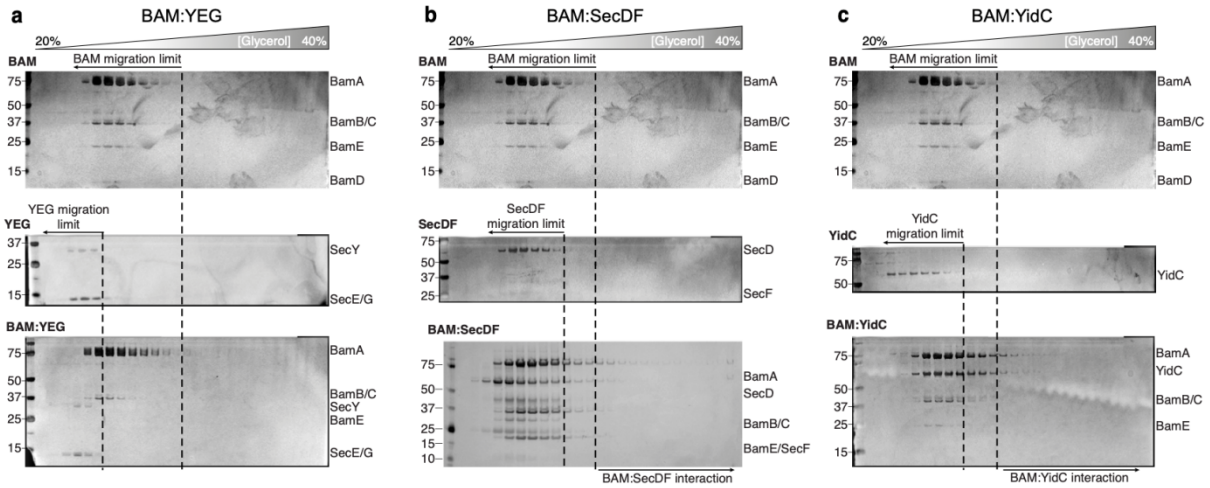

Supplementary figure 2: Glycerol centrifugation gradients of HTL and BAM components

a, b, c. Silver-stained SDS-PAGE gels of fractions from the glycerol centrifugation gradients are shown, with increasingly large complexes appearing in fractions of higher percentage glycerol, (from left to right). For each panel, the glycerol centrifugation gradient of BAM alone is shown (top). The middle gel represents a HTL component (labelled on the top left of the gel). The bottom gel represents the experiment where BAM was mixed with the corresponding HTL component. Dashed lines represent the fraction of furthest migration of the individual components, as determined in the top two gels.

1274

1275

1276

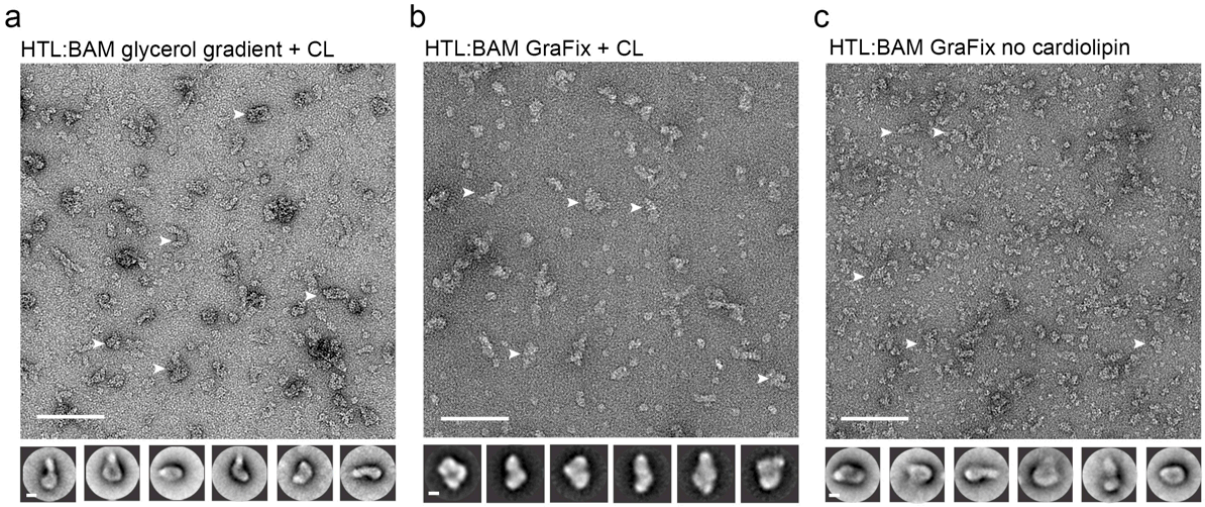

1277

1278 **Supplementary figure 3: Negative-stained EM micrographs of the HTL:BAM complex**

1279

1280 **a, b, c.** Electron micrographs of HTL-BAM complexes in different conditions. Bottom, reference-
1281 free (RF) class averages of the largest populations found in the micrographs (top). Micrograph
1282 scale bar, 1000 Å. RF scale bar, 100 Å. White arrows indicate representative HTL:BAM
1283 complexes used for image processing.

1284

1285

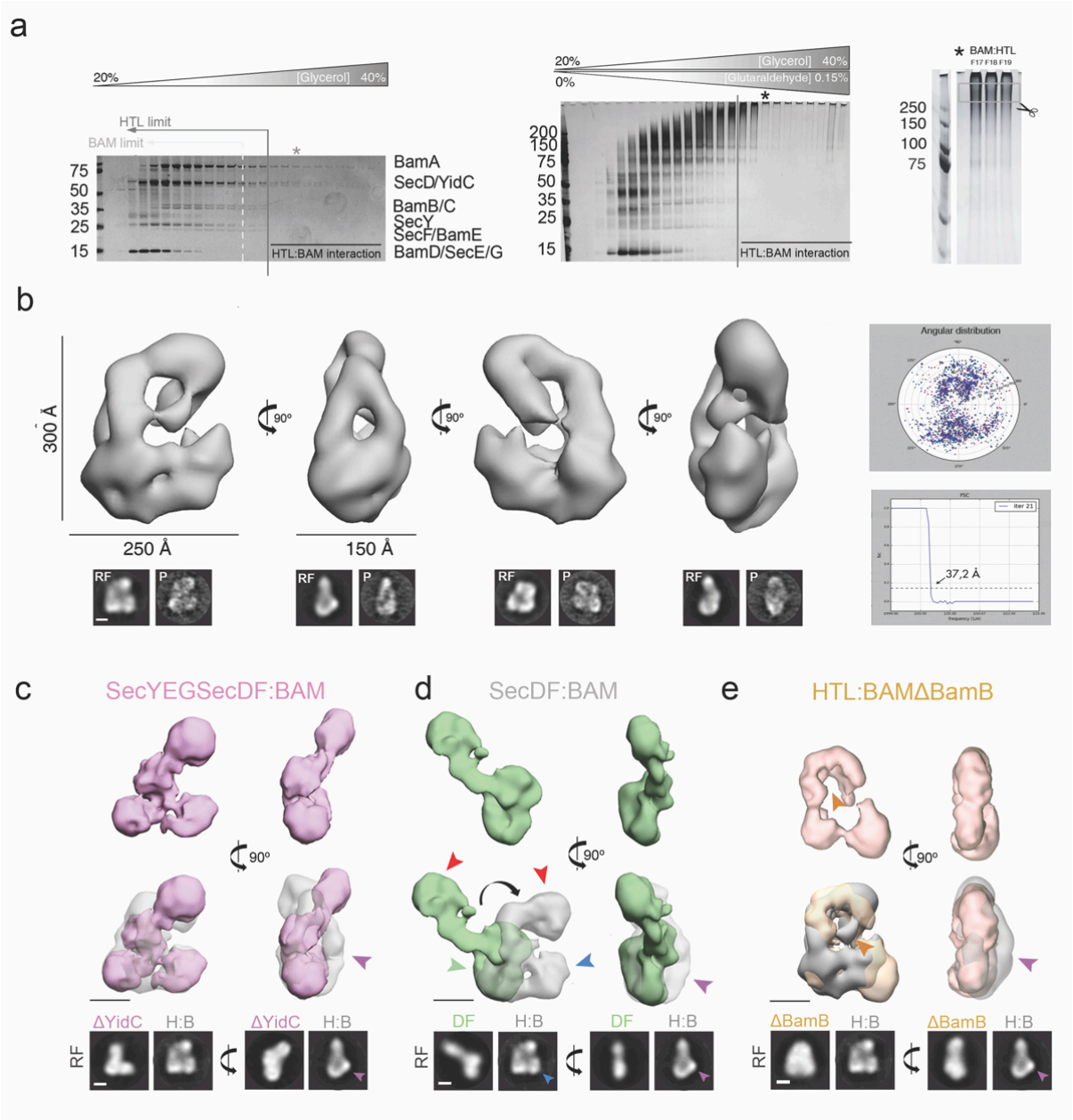
a
20%
[Glycerol] 40%
HTL limit
BAM limit
75
50
35
25
15
HTL:BAM interaction
BamA
SecD/YidC
BamB/C
SecY
SecF/BamE
BamD/SecE/G
20%
[Glycerol] 40%
0%
[Glutaraldehyde] 0.15%
200
150
75
50
35
25
15
HTL:BAM interaction
BAM:HTL
F17 F18 F19
250
150
100
75
b
300 Å
90°
250 Å
150 Å
RF
P
Angular distribution
FSC
iter 21
37,2 Å
c
SecYEGSecDF:BAM
ΔYidC
H:B
d
SecDF:BAM
DF
e
HTL:BAMΔBamB
ΔBamB

1295

1296

1297 **Supplementary figure 4: 3D characterization and subunit assignment of HTL-BAM by**
1298 **NS-EM in detergent solution**

1299

1300 **a.** Silver stained SDS-PAGE analysis of HTL-BAM fractionated by glycerol density gradient
1301 centrifugation (left), and the same but with GraFix treatment (middle). Lines show the limit to
1302 which BAM (dashed white line) and HTL (solid black line) migrate when ran alone (Fig. 2a).
1303 Asterisk (middle panel) shows the fraction chosen for MS (Table S1), EM and image
1304 processing. Right panel, silver stain SDS-PAGE gel showing fractions and bands used for
1305 analysis by mass spectrometry.

1306

1307 **b.** Top left, four orthogonal views of the HTL-BAM complex 3D reconstruction (37.2 Å
1308 resolution). Bottom, reference-free (RF) class averages and projections (P) of the final model,
1309 shown in the same orientations as the top. Scale bar, 100 Å. See Table S2 for image processing
1310 details. Right, angular distribution and Fourier shell correlation of the HTL-BAM complex.

1311

1312 For **(c-e)**, top panel shows orthogonal views of different 3D reconstructions, labelled
1313 accordingly. Middle panel shows reconstructions superimposed with HTL-BAM (transparent
1314 grey) from **(b),** and bottom shows a comparison of the reference-free (RF) class averages of
1315 HTL-BAM with the corresponding structure. Scale bar, 100 Å. See Table S2 for image
1316 processing details.

1317

1318 **c.** SecYEG-SecDF-BAM (without YidC) complex 3D reconstruction (36.7 Å resolution, pink).
1319 Pink arrow indicates the mass in HTL-BAM (grey transparent) corresponding to YidC.

1320

1321 **d**. SecDF-BAM (without SecYEG and YidC) complex 3D reconstruction (39.4 Å resolution,
1322 green). Masses for SecDF trans-membrane domain (green arrow) and periplasmic region (red
1323 arrow), SecYEG (blue arrow) and YidC (pink arrow) are indicated.

1324

1325 **e**. HTL-BAM(ΔBamB) complex 3D reconstruction (33.6 Å resolution, orange). Mass
1326 corresponding to BamB (orange arrow) and YidC (pink arrow) are indicated.
1327
1328

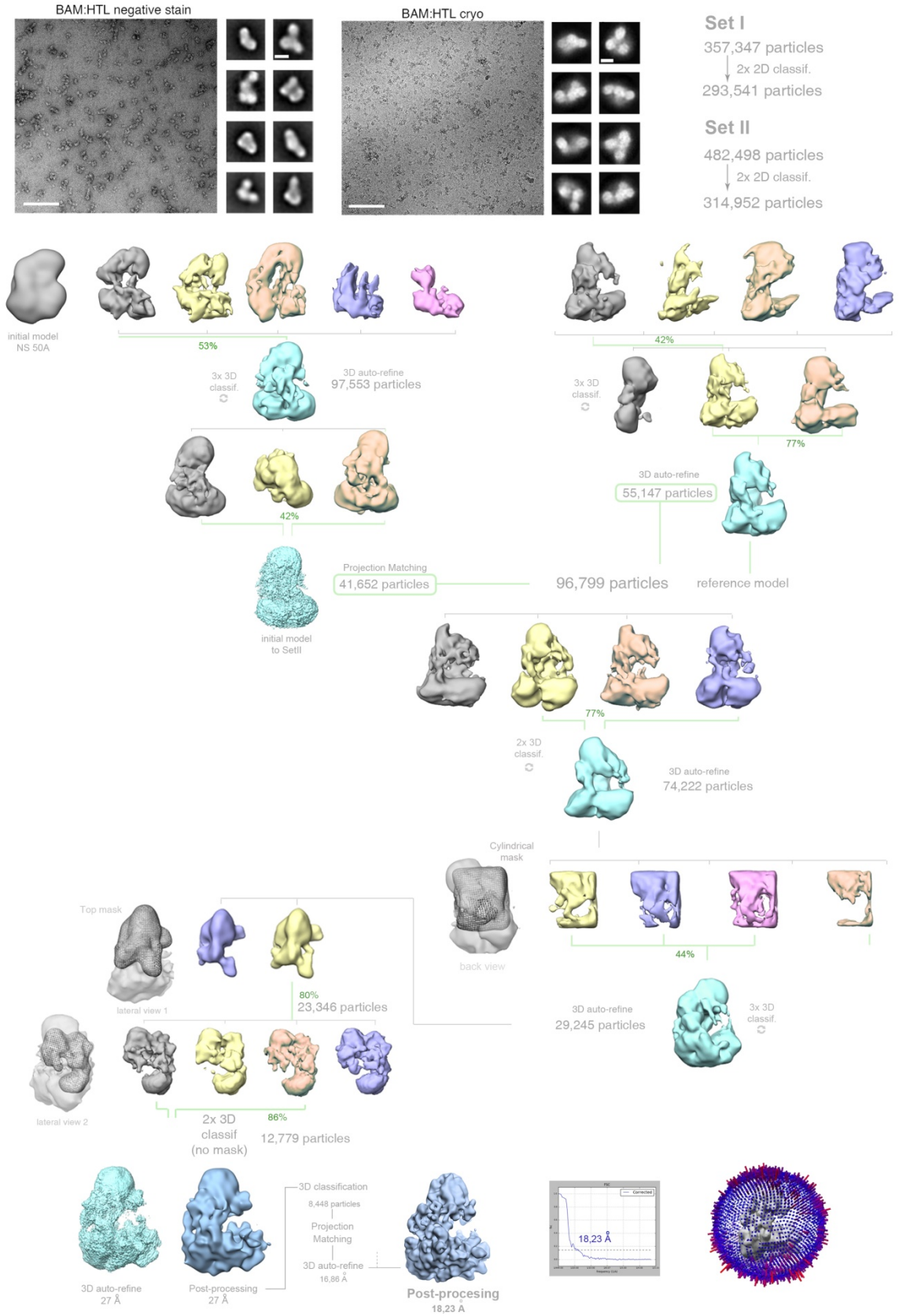
BAM:HTL negative stain
BAM:HTL cryo
Set I
357,347 particles
2x 2D classif.
293,541 particles
Set II
482,498 particles
2x 2D classif.
314,952 particles
initial model NS 50A
53%
3x 3D classif.
3D auto-refine
97,553 particles
42%
Projection Matching
41,652 particles
initial model to SetII
42%
3x 3D classif.
77%
3D auto-refine
55,147 particles
96,799 particles
reference model
77%
2x 3D classif.
3D auto-refine
74,222 particles
Cylindrical mask
back view
44%
3D auto-refine
29,245 particles
3x 3D classif.
Top mask
lateral view 1
80%
23,346 particles
lateral view 2
2x 3D classif (no mask)
86%
12,779 particles
3D auto-refine
27 Å
Post-processing
27 Å
3D classification
8,448 particles
Projection Matching
3D auto-refine
16,86 Å
Post-processing
18,23 Å
18,23 Å

1329

1330

1331 **Supplementary figure 5: <u>Image processing and classification strategy for the cryo-EM data</u>**
1332 **<u>of the HTL-BAM</u> complex**

1333

1334 Relion 2D classification was used to clean the two preliminary datasets and classify the images.
1335 Of Set I, 82% of the particles were used for extensive 3D classifications and auto-refinements. Of
1336 Set II, 65% of the particles followed same procedure. High-quality particles from both data sets
1337 were grouped and classified again masking the most variable regions. The final stable volume was
1338 formed by 8,448 particles (1.3% of the particles): indicative of the number of different sub-
1339 populations found in the sample. The final post-processing structure (Relion 2.0) has an overall
1340 resolution of 18,23 Å.

1341
1342
1343
1344
1345
1346
1347
1348
1349
1350
1351
1352
1353
1354

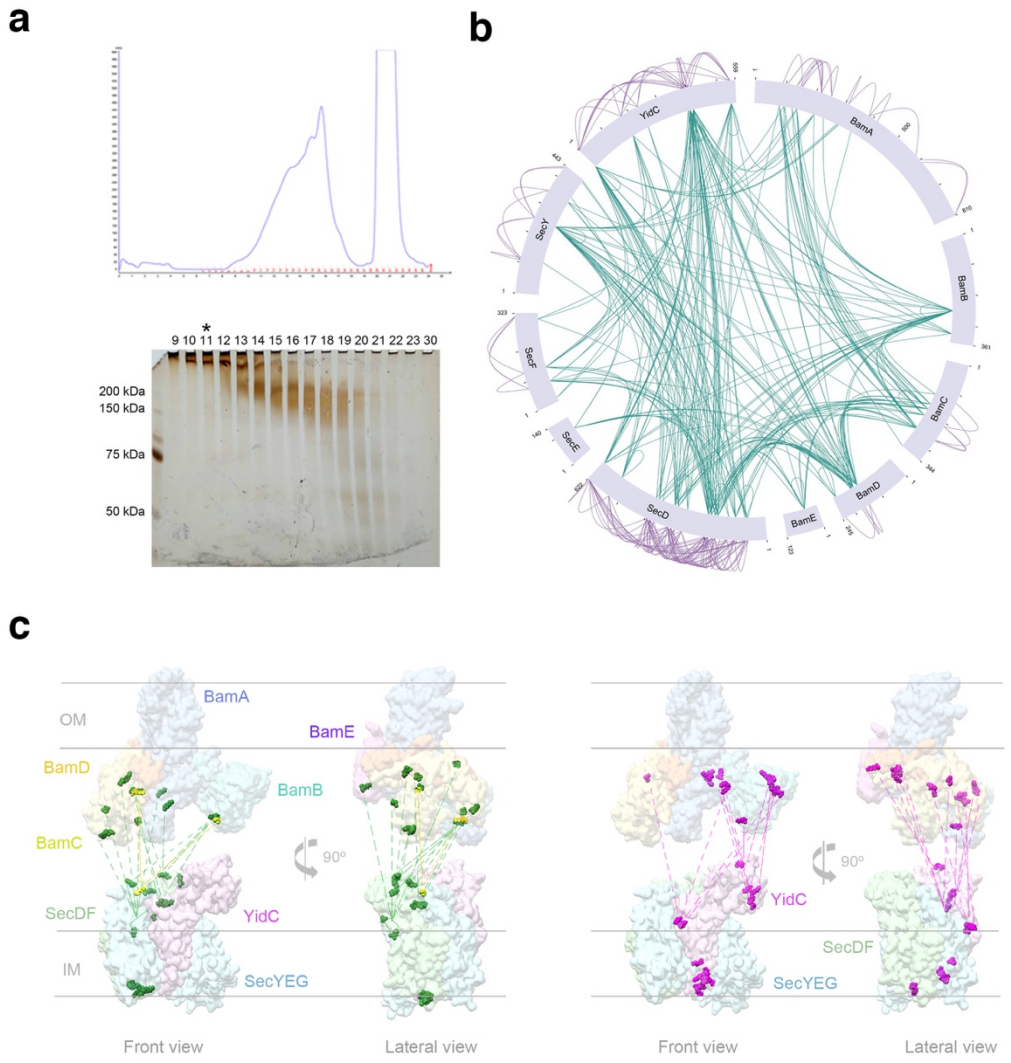
a
b
c
9 10 11 12 13 14 15 16 17 18 19 20 21 22 23 30
200 kDa
150 kDa
75 kDa
50 kDa
YidC
BamA
BamB
BamC
BamD
BamE
SecD
SecE
SecF
SecY
OM
IM
SecYEG
SecDF
90°
Front view
Lateral view

1355
1356

1357 **Supplementary figure 6: Sample preparation and XL-MS analysis of HTL-BAM**
1358
1359 **a.** Top, Gel filtration chromatography profile elution (Superose 6) of the HTL-BAM complex for
1360 cryo-EM and XL-MS analysis. Bottom, SDS-PAGE gel silver stained of the fractions eluted from
1361 the gel filtration at the top.
1362
1363 **b.** Representation of the interactome network between HTL and BAM resulted from XL-MS
1364 analysis. Internal green lines represent inter-connections between HTL-HTL, HTL-BAM and
1365 BAM-BAM components. Purple lines represent intra-connections between the HTL and BAM
1366 individual subunits.
1367
1368 **c.** Representation of inter-protein interactions between HTL and BAM as determined by XL-MS.
1369 The specific crosslinks residues are mapped onto the structures of the BAM complex (emd_4061
1370 and pdb_5ayw) and the model of the HTL complex (emd_3506 and pdb_5mg3) (Botte et al., 2016).
1371 Left, green dots and dashed lines represent positions and interactions, respectively, between SecD
1372 residues and BAM components. Yellow, positions and interactions between SecF and BAM
1373 components. Right, pink dots and dashed lines represent positions and interactions, respectively,
1374 between YidC residues and BAM components. The HTL and BAM structures have been placed
1375 artificially separate from one another to best illustrate the cross-linking contacts (rather than to
1376 reflect their actual position in the super-complex).
1377
1378
1379
1380

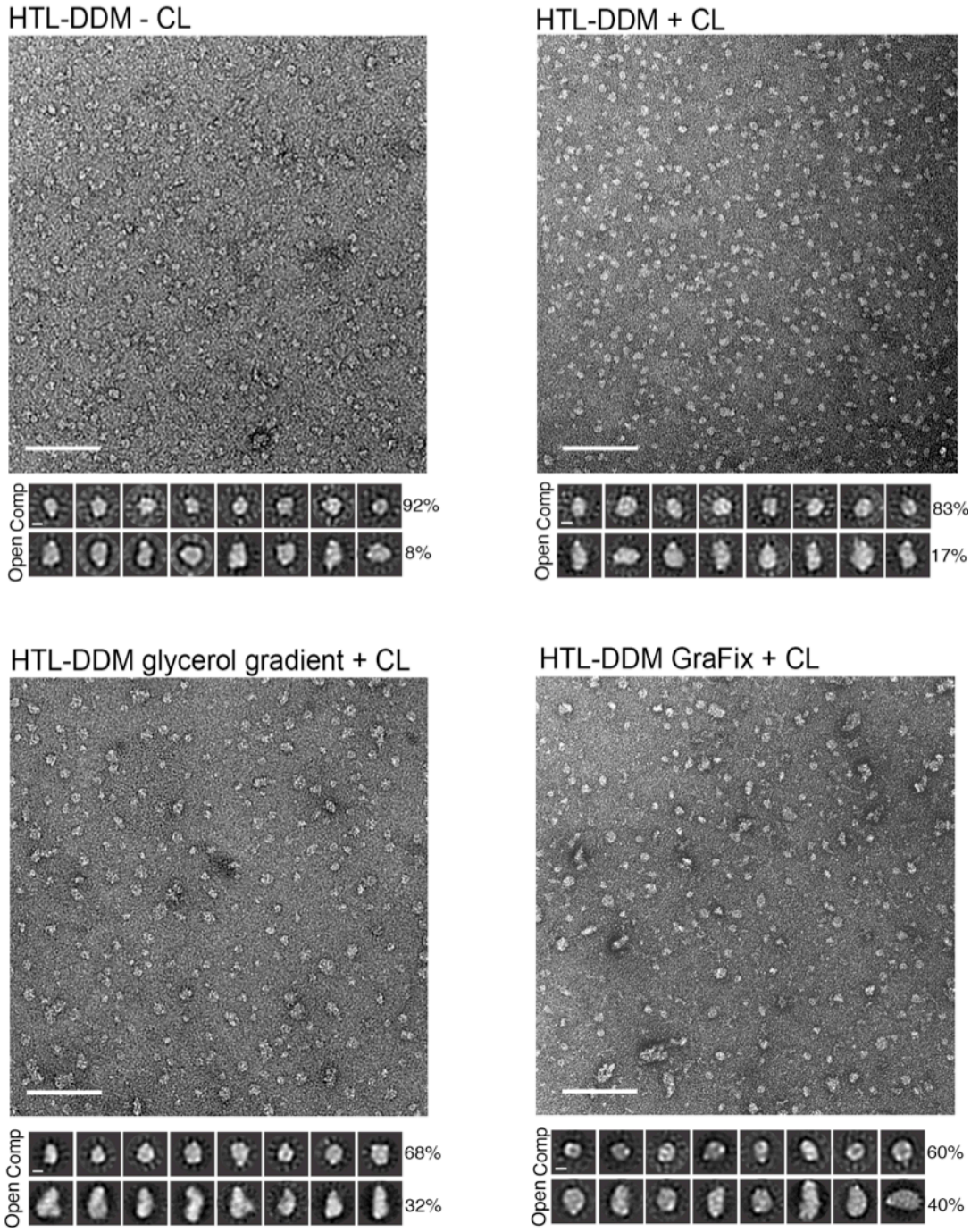

Supplementary figure 7: EM field of wild-type HTL in different conditions

Bottom, reference-free (RF) class averages of the 'compact' (comp) and 'open' populations found in the micrographs; conditions as labelled. Percentages of the populations are indicated on the right RF images. Micrograph scale bar, 1000 Å. RF scale bar, 100 Å.

1388

1389

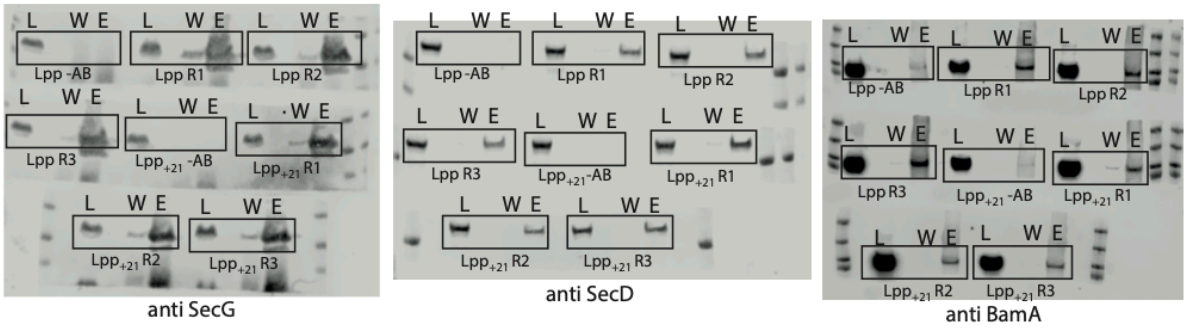

1390

1391 **Supplementary figure 8: Raw western blots of IPs investigating how periplasmic width**

1392 **effects the HTL-BAM interaction**

1393

1394 Legend is the same as described for Fig. S1a, but the cell strains used here were either *E. coli*

1395 containing WT *lpp* or the mutant lpp_{+21}. All IPs were conducted in the presence of cardiolipin.

1396

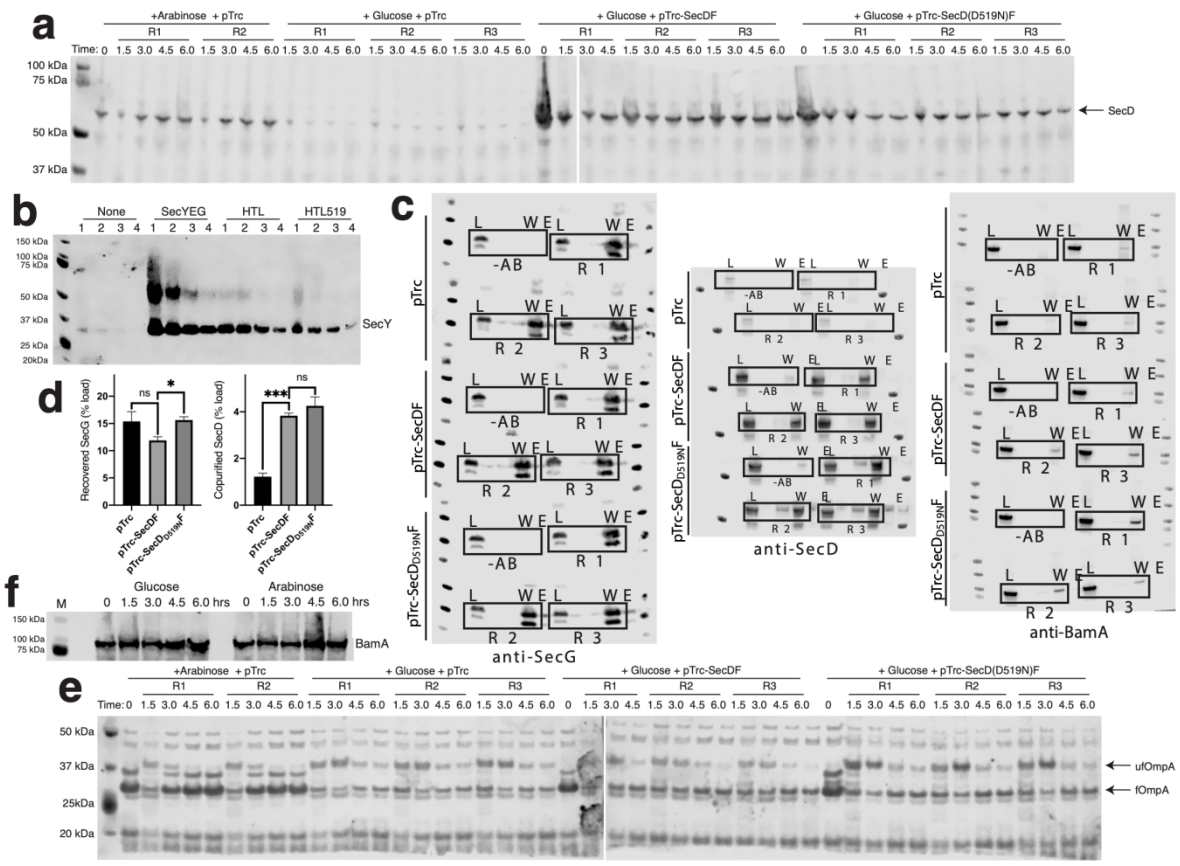
a
+Arabinose + pTrc
+ Glucose + pTrc
+ Glucose + pTrc-SecDF
+ Glucose + pTrc-SecD(D519N)F
R1
R2
R3
Time: 0 1.5 3.0 4.5 6.0
100 kDa
75 kDa
50 kDa
37 kDa
SecD
b
None
SecYEG
HTL
HTL519
150 kDa
100 kDa
75 kDa
50 kDa
37 kDa
25 kDa
20kDa
SecY
d
Recovered SecG (% load)
Copurified SecD (% load)
ns
*
***
pTrc
pTrc-SecDF
pTrc-SecD$_{D519N}$F
c
L W E
-AB
R 1
R 2
R 3
anti-SecG
anti-SecD
anti-BamA
f
M
Glucose
Arabinose
0 1.5 3.0 4.5 6.0 hrs
BamA
e
ufOmpA
fOmpA

1413

1414

1415 **Supplementary figure 9: Raw western blots accompanying SecD depletion experiments**
1416 **from Fig. 5**

1417

1418 **a.** Western blots of whole cells visualised for SecD. Cell strains used were *E. coli* JP325
1419 containing either empty pTrc99a, pTrc99a-SecDF or pTrc99a-SecD$_{D519N}$F. Samples were
1420 grown in either arabinose (permissive) or glucose (non-permissive), as indicated in the figure.
1421 R1/2/3 represent samples taken from replicate cultures. These blots were quantified to give Fig.
1422 5f.

1423

1424 **b.** Immunoblotting of SecY in inverted membrane vesicles used in Fig. 5c. Samples were
1425 prepared at 4 dilutions: neat (1), ½ (2), ¼ (3) and 1/8 (4). SecY is indicated at the expected
1426 apparent Mw of 30 kDa. A higher band is also present at approximately 50 kDa, likely due to
1427 SecY dimers.

1428

1429 **c**. Raw western blots of co-IPs conducted in Fig. 5e-f. Legend is the same as for Fig. S1a, except
1430 the membranes used here were the same as those described in **(a)**, all grown in the presence of
1431 glucose for depletion of genome encoded SecDF-yajC. All IPs were conducted in the presence
1432 of cardiolipin.

1433

1434 **d**. Quantification of SecG and SecD from co-IPs shown in **(c)**. An unpaired t-test was used to
1435 compare samples ($p = 0.05$, $n = 3$, * = < 0.05, *** = < 0.001, p values from left to right are
1436 0.0.1391, 0.0137, 0.0001 and 0.3618).

1437

1438 **e.** OmpA western blots of periplasmic fractions of cells from **(a).** Unfolded (ufOmpA) and
1439 folded OmpA (fOmpA) are indicated. These blots were quantified to give Fig. 5i.

1440

1441 **f.** BamA western blot of whole cells taken from cultures grown during depletion of SecDF-
1442 yajC.

1443

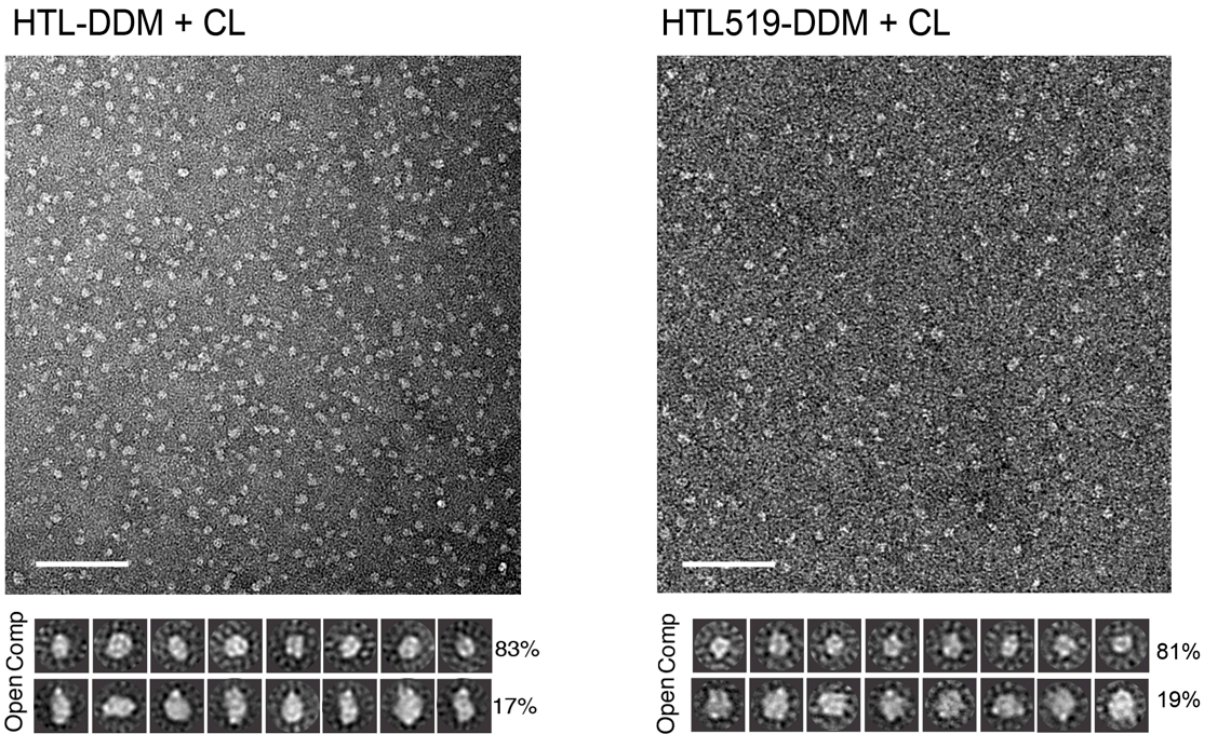

Supplementary figure 10: Negative-stain EM of HTL containing $SecD_{D519N}$ (HTL519)

Electron micrographs of wild type (wt) HTL and HTL containing $SecD_{D519N}F$ (HTL519) in the same conditions (with cardiolipin, and without GraFix). Bottom, reference-free (RF) class averages of the 'compact' (comp) and 'open' populations found in the micrographs (top). Percentages of the populations are indicated on the right of RF images. Micrograph scale bar, 1000 Å. RF scale bar, 100 Å.

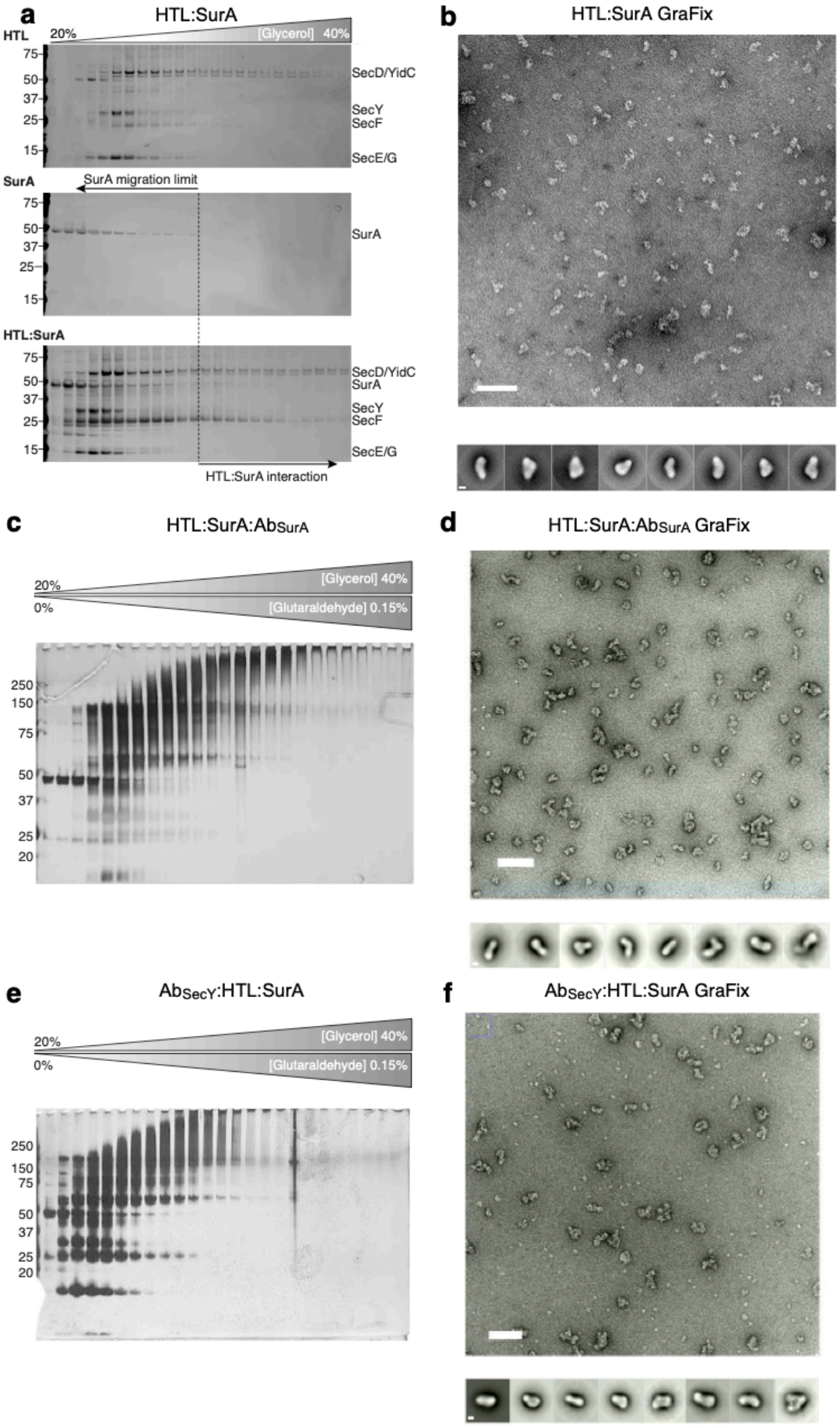
a
HTL:SurA
HTL
20%
[Glycerol] 40%
75
50
37
25
15
SecD/YidC
SecY
SecF
SecE/G
SurA
SurA migration limit
SurA
HTL:SurA
SecD/YidC
SurA
SecY
SecF
SecE/G
HTL:SurA interaction
b
HTL:SurA GraFix
c
HTL:SurA:AbSurA
20%
[Glycerol] 40%
0%
[Glutaraldehyde] 0.15%
250
150
75
50
37
25
20
d
HTL:SurA:AbSurA GraFix
e
AbSecY:HTL:SurA
20%
[Glycerol] 40%
0%
[Glutaraldehyde] 0.15%
250
150
75
50
37
25
20
f
AbSecY:HTL:SurA GraFix

1453 **Supplementary figure 11: Glycerol gradient centrifugation, electron micrographs and**
1454 **immunodecoration of HTL:SurA**
1455
1456 For **(a), (c)** and **(e)**, the experiment was conducted as in Fig. S2. EM fields of HTL:SurA (**b,** top)
1457 and HTL:SuraA:Ab_{SurA} (**d,** top) and Ab_{SecY}:HTL:SurA (**f**, top) prepared using GraFix are shown.
1458 Reference-free (RF) class averages of the biggest populations from corresponding micrographs are
1459 shown (bottom). Micrograph scale bar, 1000 Å. RF scale bar, 100 Å.
1460
1461
1462
1463
1464
1465
1466
1467
1468
1469
1470
1471
1472
1473

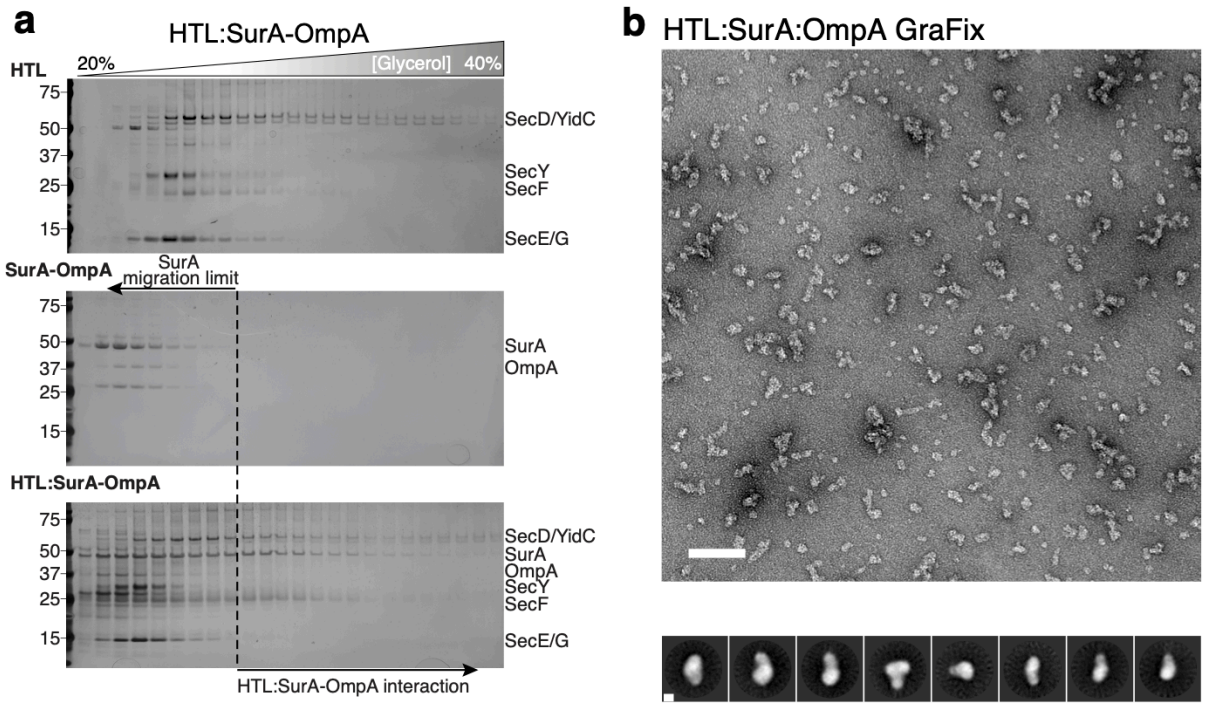

Supplementary figure 12: Negative stain EM micrograph and glycerol gradient centrifugation of HTL-SurA-OmpA

For **(a)**, the experiment was conducted as in Fig. S2. An EM field of HTL:SurA:OmpA prepared using GraFix is shown (**b**). Reference-free (RF) class averages of the biggest populations from the micrograph is shown (bottom). Micrograph scale bar, 1000 Å. RF scale bar, 100 Å.

1483

Sample		Accession	Description	Score	Coverage	rote	Peptid	# PSMs	Area
BAM:HTL detergent		B7UJN1	Protein translocase subunit SecD OS=Escherichia coli O127:H6 (strain E2348/69 / EPEC) OX=574521 GN=secD PE=3 SV=1 - [B7UJN1_ECO27]	1166.56	53.01	1	35	403	4.609E+8
		B7UIM2	Outer membrane protein assembly factor BamA OS=Escherichia coli O127:H6 (strain E2348/69 / EPEC) OX=574521 GN=bamA PE=3 SV=1 - [BAMA_ECO27]	683.99	60.74	1	46	257	7.500E+7
		B7UGM7	Outer membrane protein assembly factor BamC OS=Escherichia coli O127:H6 (strain E2348/69 / EPEC) OX=574521 GN=nlpB PE=3 SV=1 - [B7UGM7_ECO27]	404.02	55.81	1	14	119	3.642E+7
		B7UJN2	Protein-export membrane protein SecF OS=Escherichia coli O127:H6 (strain E2348/69 / EPEC) OX=574521 GN=secF PE=3 SV=1 - [B7UJN2_ECO27]	249.64	27.55	1	7	74	2.772E+7
		B7UMH2	Membrane protein insertase YidC OS=Escherichia coli O127:H6 (strain E2348/69 / EPEC) OX=574521 GN=yidC PE=3 SV=1 - [YIDC_ECO27]	181.06	36.31	1	13	64	3.983E+7
		B7UH30	Outer membrane protein assembly factor BamD OS=Escherichia coli O127:H6 (strain E2348/69 / EPEC) OX=574521 GN=yfiO PE=3 SV=1 - [B7UH30_ECO27]	173.40	66.12	1	15	76	3.235E+7
		B7UGV8	Outer membrane protein assembly factor BamB OS=Escherichia coli O127:H6 (strain E2348/69 / EPEC) OX=574521 GN=yfgL PE=3 SV=1 - [B7UGV8_ECO27]	129.35	34.44	1	11	45	3.143E+7
		B7UK24	Protein translocase subunit SecY OS=Escherichia coli O127:H6 (strain E2348/69 / EPEC) OX=574521 GN=secY PE=3 SV=1 - [B7UK24_ECO27]	36.43	15.58	1	5	14	3.454E+6
SurA:HTL detergent		B7UJN1	Protein translocase subunit SecD OS=Escherichia coli O127:H6 (strain E2348/69 / EPEC) OX=574521 GN=secD PE=3 SV=1 - [B7UJN1_ECO27]	1098.08	50.57	1	33	393	6.386E+8
		B7UMH2	Membrane protein insertase YidC OS=Escherichia coli O127:H6 (strain E2348/69 / EPEC) OX=574521 GN=yidC PE=3 SV=1 - [YIDC_ECO27]	266.32	32.66	1	13	98	1.235E+8
		B7UJN2	Protein-export membrane protein SecF OS=Escherichia coli O127:H6 (strain E2348/69 / EPEC) OX=574521 GN=secF PE=3 SV=1 - [B7UJN2_ECO27]	236.81	18.27	1	5	70	4.934E+7
		B7UIA1	Chaperone SurA OS=Escherichia coli O127:H6 (strain E2348/69 / EPEC) OX=574521 GN=surA PE=3 SV=1 - [B7UIA1_ECO27]	49.97	23.60	1	10	23	3.360E+6
		B7UK24	Protein translocase subunit SecY OS=Escherichia coli O127:H6 (strain E2348/69 / EPEC) OX=574521 GN=secY PE=3 SV=1 - [B7UK24_ECO27]	7.01	4.51	1	3	4	1.931E+6

1484

1485

1486 **Table 1: Mass spectrometry analysis of the GraFix fractions for image processing**

1487

1488 Analysis of the protein composition of the HTL-BAM and HTL-SurA preparations in detergent
1489 solution by MS. Only proteins of interest are shown in this table. The SDS-PAGE bands
1490 corresponding to the GraFix fractions used for NS-EM processing (*e.g.* Fig. S4a, middle and right,
1491 asterisk) were cut from the gel and prepared for protein digestion, extraction and MS.

1492

1493

1494

	Complex	Initial particles	High quality particles	Final 3D volume	Resolution
HTL structures	HTL-DDM	100754	74070	-	-
	HTL-DDM+CL	22869	18674	-	-
	HTLafter gradient+CL	21735	18434	-	-
	HTLafter gradient+gluta.+CL	101142	90432	9656 (compact conformation)	26,56 Å
				1569 (extended conformation)	39,54 Å
	$HTL519_{D519N}$	42098	38052	20699 (compact conformation)	18,7 Å
				4451 (extended conformation)	20,70 Å
HTL-BAM structures	HTL:BAM Δgluta	29336	12460	-	-
	HTL:BAM grafix	65381	28646	5122	37,2 Å
	HTL:BAM grafix ΔCL	14530	11406	-	-
	HTL:BAM CryoEM	839845	608493	12779	18,23 Å
	SecDF:BAM	22642	11987	5430	39,4 Å
	HTLΔYidC:BAM	16008	8612	4943	36,7 Å
	HTL:BAMΔB	31561	11484	3919	33,65 Å
HTL-SurA structures	SurA:HTL	24252	18696	2290	41,88 Å
	$SurA:HTL:Ab_{SecY}$	15819	9510	4431	47,06 Å
	Ab_{SurA}:SurA:HTL	14246	3882	730	56,67 Å
	SurA:HTL:OmpA	35546	33485	11699	37,50 Å

Table 2: Parameters of EM analysis of HTL, HTL-BAM and HTL-SurA structures